Deriving structural information from experimentally measured data on biomolecules: a review

W. F. van Gunsteren[1,*], J. R. Allison[2], X. Daura[3], J. Dolenc[1], N. Hansen[4], A. E. Mark[5], C. Oostenbrink[6], V. H. Rusu[1], L. J. Smith[7]

[1]Laboratory of Physical Chemistry, Swiss Federal Institute of Technology, ETH, Zürich, Switzerland.

[2]Centre for Theoretical Chemistry and Physics & Institute of Natural and Mathematical Sciences, Massey University, Auckland, New Zealand.

Biomolecular Interaction Centre, University of Canterbury, Christchurch, New Zealand.

Maurice Wilkinson Centre for Molecular Biodiscovery, New Zealand.

[3]Institute of Biotechnology and Biomedicine, Universitat Autonoma de Barcelona (UAB), 08193, Barcelona, Spain.

Catalan Institution for Research and Advanced Studies (ICREA), 08010, Barcelona, Spain

[4]Institute of Thermodynamics and Thermal Process Engineering, University of Stuttgart, Pfaffenwaldring 9, 70569, Stuttgart, Germany.

[5]School of Chemistry and Molecular Biosciences, University of Queensland, St. Lucia, QLD 4072, Australia

[6]Institute of Molecular Modeling and Simulation, University of Natural Resources and Life Sciences, Vienna, Austria.

[7]Department of Chemistry, University of Oxford, Inorganic Chemistry Laboratory, South Parks Road, Oxford OX1 3QR, United Kingdom.

Submitted to:

Angew. Chemie

Manuscript ID:

Date:

July 4, 2016

---

[*]Corresponding author. Email: `wfvgn@ethz.ch`

Abstract

During the past half century, the number and accuracy of experimental techniques that can deliver values of observables for biomolecular systems have been steadily increasing. The conversion of a measured value Q^{exp} of an observable quantity Q into structural information is, however, a task beset with theoretical and practical problems: (i) insufficient or inaccurate values of Q^{exp}, (ii) inaccuracies in the function $Q(\vec{r})$ used to relate the quantity Q to structure $\vec{r}$, (iii) how to account for the averaging inherent in the measurement of Q^{exp}, (iv) how to handle the possible multiple-valuedness of the inverse $\vec{r}(Q)$ of the function $Q(\vec{r})$, to mention a few. These apply to a variety of observable quantities Q and measurement techniques such as X-ray and neutron diffraction, small-angle and wide-angle X-ray scattering, free-electron laser imaging, cryo-electron microscopy, nuclear magnetic resonance, electron paramagnetic resonance, infrared and Raman spectroscopy, circular dichroism, Förster resonance energy transfer, atomic force microscopy and ion-mobility mass spectrometry. The process of deriving structural information from measured data is reviewed with an eye to non-experts and newcomers in the field using examples from the literature of the effect of the various choices and approximations involved in the process. A list of choices to be avoided is provided.

1 Introduction

Over the past half century it has become increasingly feasible to obtain structural information on biomolecules at the atomic level of resolution due to the development of a range of experimental techniques.

1. The analysis of X-ray diffraction patterns can be used to the elucidate the spatial structure of proteins.[1–3]

2. Neutron diffraction measurements can be used to determine the positions of hydrogen (i.e. deuterium) atoms,[4] and provide information complementary to X-ray diffraction.

3. Small-angle X-ray scattering (SAXS) and wide-angle X-ray scattering (WAXS) can be used to derive low resolution structural constraints for large biomolecules.[5]

4. Free-electron X-ray lasers may be used for coherent imaging of biomolecules.[6, 7]

5. Cryo-electron microscopy can provide structural information approaching that of X-ray crystallography.[8]

6. One- and higher-dimensional NMR techniques[9] can be used to obtain atom-atom distances within molecules, which in turn can be used to derive spatial structures for biomolecules.[10]

7. Electron Paramagnetic Resonance (EPR) measurements yield long-range distance information between particular types of atoms.[11]

8. Infrared (IR), Raman and fluorescence spectroscopy can be used to derive local structural information on proteins.[12, 13]

9. Circular Dichroism (CD) can provide information on secondary structure content of a protein fold, but spectra possess a much lower information density than can be obtained by NMR spectroscopic or X-ray diffraction techniques.[14]

10. Förster Resonance Energy Transfer (FRET) can be used to trace distances between particular moieties attached to biomolecules.[15–17]

11. Atomic Force Microscopy (AFM) can be used to obtain mechanical or electrical response functions regarding particular systems.[18]

12. Ion-mobility mass spectrometry (IM-MS) yields collision cross sections that can be used to obtain size and shape information on biomolecules in the gas phase.[19]

A number of quantities Q, which are related to the mentioned measurement techniques and for which values can be more or less directly measured, are listed in Table 1.

In order to extend our understanding of biomolecular processes at the atomic level of resolution the measured values of Q^{exp} of an observable quantity $Q(\vec{r}^N, \vec{p}^N)$ that depends on the Cartesian coordinates $\vec{r}^N \equiv (\vec{r}_1, \vec{r}_2, \ldots, \vec{r}_N)$ and conjugate momenta $\vec{p}^N \equiv (\vec{p}_1, \vec{p}_2, \ldots, \vec{p}_N)$ of the N atoms in the molecular system, must be converted into spatial, structural and dynamical information in terms of the statistical-mechanical phase-space variables $\vec{r}^N$ and $\vec{p}^N$ of the system. The quantities $Q(\vec{r}^N, \vec{p}^N)$ listed in Table 1 primarily depend on the atomic coordinates $\vec{r}^N$. For this reason and for simplicity, the dependence of Q on the momenta $\vec{p}^N$ will not be discussed further.

If the molecules in the system move, the value $Q(\vec{r}^N(t))$ becomes depen-

Table 1: Some quantities Q and their dependence on configuration $\vec{r}^N = (\vec{r}_1, \vec{r}_2, \ldots, \vec{r}_N)$ of N particles. θ denotes a torsional angle or an angle between a bond in a molecule and the direction of an applied magnetic field, and $\vec{\mu}$ an electronic transition dipole. $\hat{r} = \vec{r}/r$.

Quantity $Q(\vec{r}^N)$	Dependence of $Q(\vec{r}^N)$ on configuration $\vec{r}^N$ of N particles
Structure factors (amplitudes)	$F_{hkl}(\vec{r}^N)$
NOE intensities	$I_{i,j}(\vec{r}^N)$
distances	r_{ij}^{-p} with $p = 3$ or 6
^{3}J-coupling constants	$^3J_{i,j} = a\cos^2\theta_{i,j} + b\cos\theta_{i,j} + c$
Residual dipolar couplings	$D_{i,j} = a\cos^2\theta_{i,j} + b$
S^2 order parameters	$S^2_{i,j} = \frac{1}{2}\left\{3\sum_{\alpha=1}^{3}\sum_{\beta=1}^{3}\left\langle\frac{\hat{r}_{ij_\alpha}\hat{r}_{ij_\beta}}{r_{ij}^3}\right\rangle^2 - \left\langle\frac{1}{r_{ij}^3}\right\rangle^2\right\}$
Chemical shielding	$\sigma(\vec{r}^N)$
FRET efficiencies	$E_{DA} = E(\vec{\mu}_D, \vec{\mu}_A, r_{DA})$
CD spectra	$I(\lambda; \vec{r}^N)$

dent on time. Depending on the type of measurement technique used, a measured value of $Q^{\exp}$ of an observable quantity Q corresponds to an average over molecules in the system and over the time period of the measurement. Different experimentally measured quantities will be sensitive to different time windows. For example, NMR implicitly performs time averaging due to the finite duration of the various radio-frequency pulses and mixing times as well as the nature of the specific phenomenon measured, e.g. magnetisation transfer. In a NMR Nuclear Overhauser Effect (NOE) measurement the time window of sensitivity depends on the rotational tumbling time and thus on the size and the solvent environment of the molecule of interest. Such a time window of sensitivity may in some cases be used to infer the time scale of particular molecular motions.

However, for most biomolecular systems studied the measured values Q^{exp} are used to derive structural information on biomolecules that is independent of time.

A value $Q(\vec{r}^N)$ for a particular configuration $\vec{r}^N$ can be calculated using theory that connects an observable Q to electronic and nuclear coordinates and properties of molecules. For example, the intensity I_{hkl} of a diffracted X-ray beam as function of the crystal lattice or Miller indices h, k and l can be obtained as the square of the structure factor amplitude $F_{hkl}(\vec{r}^N)$ that results from a spatial Fourier transform of the electron density of the system.[20] NOE intensity $I_{i,j}(\vec{r}^N)$ for a pair of nuclear spins belonging to atoms i and j can be obtained by a relaxation matrix calculation.[21] ${}^3J_{i,j}$-couplings between atoms i and j connected by three covalent bonds can be estimated using the Karplus relation[22] with its coefficients a, b and c commonly empirically determined from chosen data sets of ${}^3J$-coupling values and molecular structures.[23] The chemical shielding $\sigma_i(\vec{r}^N)$ for an atom i is related to the local electron density which can in principle be calculated quantum-chemically. However for proteins empirical relations are currently commonly used.[24] These are based on fitting calculated chemical shifts to measured ones for a chosen set of molecules and structures.

In order to obtain a value $Q(\vec{r}^N)$ from a molecular configuration $\vec{r}^N$, generally the following procedure is followed.[25]

1. The atomic, electronic or nuclear degrees of freedom $\vec{r}$ of the solute or solvent essential to describe the relation $Q(\vec{r}^N)$ are determined. For example, a ${}^3J_{i,j}$-coupling between the spins of atoms i and j depends primarily on the torsional angle $\theta_{i,j}$ defined by the four covalently connected atoms

$i - k - l - j$.

2. A relation $Q(\vec{r}^N)$ between Q and a particular configuration $\vec{r}$ is postulated. This may be based on quantum-chemical theory, empirical relations or a combination of both. For example, the form of the Karplus relation $Q(\vec{r}) = {}^3J(\theta)$ follows from quantum-chemical considerations, but its parameters a, b and c are empirically determined. Such a relation or function $Q(\vec{r})$ generally involves a variety of assumptions and approximations, which determine its accuracy.[26]

3. An empirical interaction function $V^{\mathrm{phys}}(\vec{r}^N)$ or force field that governs the statistical-mechanical distribution of configurations $\vec{r}^N$ is then used to generate an ensemble of configurations $\vec{r}^N$ with probability of occurrence $P(\vec{r}^N)$. For example, at constant temperature T a Boltzmann-weighted ensemble with configurational probability

$$P(\vec{r}^N) = \frac{\exp\left(-V^{\mathrm{phys}}(\vec{r}^N)/(k_{\mathrm{B}}T)\right)}{\int \exp\left(-V^{\mathrm{phys}}(\vec{r}^N)/(k_{\mathrm{B}}T)\right) \mathrm{d}\vec{r}^N}, \tag{1}$$

is normally required, where k_{B} denotes Boltzmann's constant.

4. Either equations of motion for the atoms in the system can be integrated as function of time[27] or an alternative method to generate an ensemble of Boltzmann-weighted configurations can be chosen.

5. The ensemble average

$$\langle Q \rangle_{\mathrm{sim}} \equiv \langle Q \rangle_{\vec{r}^N} \equiv \int Q(\vec{r}^N) P(\vec{r}^N) \mathrm{d}\vec{r}^N, \tag{2}$$

is then calculated and compared to the measured value $Q^{\mathrm{exp}} \equiv \langle Q \rangle_{\mathrm{time,space}}$,

which is normally an average, over time and a set of molecules.

If $V^{\mathrm{phys}}(\vec{r}^N)$ and $Q(\vec{r}^N)$ are correct, i.e. they correspond exactly to reality, and the sampling of configurations $\vec{r}^N$ is infinite, one would find,

$$\langle Q \rangle_{\mathrm{sim}} = Q^{\mathrm{exp}}, \tag{3}$$

that is there is an exact match between simulation and experiment. Assuming Q^{exp} is correct further experiments would no longer be needed. However, in practice these four conditions are rarely satisfied. This leads to the question how to derive a structure or rather a set of structures, $\vec{r}^N$, from a set of measured values Q^{exp}.

When trying to derive a structure $\vec{r}^N$ from Q^{exp} values the following problems are generally encountered.

1. For most biomolecular systems the number of independent Q^{exp} values available is much smaller than the number of degrees of freedom of the system. This means the problem is underdetermined.

2. Q^{exp} values contain uncertainty or error.

3. It is not possible to fully account for averaging over time and space inherent in the experimental measurement: inversion of the averaging operation in Eq. 2 is impossible.

4. The function $Q(\vec{r})$ is not known or the accuracy of the function is uncertain.

5. The inverse $\vec{r}(Q)$ of the function $Q(\vec{r})$ may not exist or if it does, it may be multiple-valued, as in the case of the Karplus relation.

6. The sampling of configurations $\vec{r}^N$ must be biased, i.e. guided towards $Q^{\rm exp}$. This is especially challenging if the inverse $\vec{r}(Q)$ of $Q(\vec{r})$ is multiple-valued.

Over the past decades, this structure, i.e. ensemble determination problem has been approached in a variety of ways. While some of these approaches have a sound physical basis, others are highly speculative or ad-hoc.

Since for all but the smallest molecules in crystalline form the number of values of observable quantities in a biomolecular system is much smaller than the number of degrees of freedom of the system, virtually all procedures to derive structure $\vec{r}^N$ from $Q^{\rm exp}$ values rely on an atomic model, i.e. a function specifying likely structural parameters of a system. This normally takes the form of an atomic interaction function $V^{\rm phys}(\vec{r})$ that yields low-energy values for configurations that are physically most reasonable. Such a function can be volume-based (only atom-atom contact interactions, no long-range electrostatic or hydrogen bonding terms), such as used in the structure refinement program X-PLOR.[28] The X-PLOR refinement function contains bond-length, bond-angle, torsional-angle and atomic volume parameters, but no electrostatic terms. The quality of the set or ensemble of structures derived from the set of $Q^{\rm exp}$ values depends on (*i*) the number and accuracy of the $Q^{\rm exp}$ values; (*ii*) the accuracy of the function $V^{\rm phys}(\vec{r}^N)$ used in the structure determination procedure; and (*iii*) the validity and accuracy of the procedure that was used to derive a structure $\vec{r}^N$ from the $Q^{\rm exp}$ values.

A common way to derive a structure from measured data is to represent the latter by a biasing or restraining function $V^{Q,{\rm restr}}\left(Q(\vec{r}^N);Q^\circ\right)$ that limits the deviation of $Q(\vec{r}^N)$ from the measured target value $Q^\circ = Q^{\rm exp}$. This function

$V^{Q,\mathrm{restr}}$ is added to the physical interaction function V^{phys} used to describe the system,

$$V(\vec{r}^N) = V^{\mathrm{phys}}(\vec{r}^N) + V^{Q,\mathrm{restr}}\left(Q(\vec{r}^N); Q^\circ\right). \tag{4}$$

This function is then minimised or used in a simulation. In the early days of biomolecular structure determination, the function $V(\vec{r}^N)$ was minimised with respect to a variation of the structure $\vec{r}^N$.[29] Because molecular dynamics (MD) simulation is able to overcome energy barriers in the order of $k_\mathrm{B}T$, energy minimization was replaced by MD simulation first in structure determination based on NMR data (1983)[30,31] and later in structure determination based on X-ray diffraction data (1987).[32,33] Currently, MD simulation of biomolecular systems in which a biasing or restraining function $V^{Q,\mathrm{restr}}$ is added to V^{phys} in order to bias the sampling towards Q^{exp} values is the standard method to derive structural information from measured data.[34] The various procedures and techniques that can be applied lead to the question how best to use experimental data in biomolecular structure refinement. When using experimental data to bias the sampling, the following issues should be considered.

1. Whether the experimental information corresponds to observed as opposed to derived data.
2. Whether the number of experimental data Q^{exp} is sufficient.
3. The accuracy of the (physical) force field $V^{\mathrm{phys}}(\vec{r}^N)$.
4. The accuracy and consistency of the experimental data Q^{exp}.
5. The accuracy of the function $Q(\vec{r})$ relating observable Q to structure $\vec{r}$.
6. The choice of biasing function $V^{Q,\mathrm{restr}}(\vec{r})$ to guide $\langle Q\rangle_{\mathrm{sim}}$ towards Q^{exp}.

7. The weighting of the biasing function $V^{Q,\mathrm{restr}}(\vec{r})$ relative to that of the force field energy $V^{\mathrm{phys}}(\vec{r}^N)$ in $V(\vec{r}^N)$.

8. How to deal with averaging over time and space.

9. How to bias the sampling especially when the inverse $\vec{r}(Q)$ of the function $Q(\vec{r})$ is multiple-valued.

10. How to ensure Boltzmann sampling or weighting of configurations $\vec{r}$.

In the present manuscript these ten issues are discussed using examples pertaining to various observables Q. The examples were chosen from our own work and mainly regard observables Q for which values can be determined through NMR spectroscopy. The examples given mostly relate to small molecules and peptides in order to avoid conformational sampling deficiencies that hamper the convergence of averages in larger systems such as proteins when the conformational space that is to be sampled is too large. It should be noted, however, that the issues they illustrate also relate to all other observable quantities and measurement techniques mentioned above. The impact of choices made on the structural interpretation of experimental data is evaluated, and a list of choices to be avoided in structure refinement based on measured data is presented. Finally, the consequences of the different ways to derive biomolecular structure from experimental data for the management of structural databases such as the Protein Data Bank (PDB)[35] are considered.

2 Deriving structure from measured values of observables

The modelling techniques described are based on statistical mechanics, in which $\vec{r}^N$ corresponds to a configuration. This applies to the solute and solvent com-

bined. By grouping together slightly different configurations of a solute molecule that show particular geometric features, we refer to such a set of configurations as a conformer. For example, all configurations of a solute that possess slightly varying bond lengths and bond angles and torsional angles within a limited range, e.g. 30° from a minimun-energy angle, may be considered a single conformer. This is done when the differences between the configurations that belong to this conformer are irrelevant for the phenomenon that is observed.

2.1 Use of observed as opposed to derived "experimental" data

Quantities $Q(\vec{r}^N)$ that can be calculated from configurations $\vec{r}^N$ can be either observable quantities $Q^{\mathrm{obs}}(\vec{r}^N)$ that are directly measurable in an experiment, or non-observable quantities $Q^{\mathrm{der}}(\vec{r}^N)$ that are derived from $\langle Q^{\mathrm{obs}} \rangle_{\mathrm{exp}}$ values by applying a given procedure, f, based on various assumptions and approximations.[36]

$$Q^{\mathrm{der}} = f\left(\langle Q^{\mathrm{obs}} \rangle_{\mathrm{exp}}\right). \tag{5}$$

Peak location and intensity from X-ray diffraction or NMR spectroscopic experiments are examples of observable quantities Q^{obs}, whereas molecular structure, torsional angles, or NMR order parameters are examples of derived quantities Q^{der}. The latter reflect to some extent the assumptions and approximations associated with the procedure f used to convert $\langle Q^{\mathrm{obs}} \rangle_{\mathrm{exp}}$ into Q^{der}. Depending on the validity of the assumptions and the reliability of the approximations involved, the obtained Q^{der} values may in reality carry little experimental information. If so their use in the restraining function may lead to a flawed structural

interpretation of the $\langle Q^{\mathrm{obs}} \rangle_{\mathrm{exp}}$ values. In principle, only values Q° of observable quantities Q^{obs} should be used in the restraining function.

An example of the effect of using a flawed procedure f to derive structural restraints can be found in Ref. 37. NMR measurements of a β-octa-peptide solvated in methanol yielded 40 NOE atom-atom distance bounds and 12 ^3J-coupling constants.[38] Using single-structure refinement and the volume-based interaction function V^{phys} of the structure refinement program X-PLOR,[28] 20 NMR model structures were generated. These suggested the peptide adopted a hitherto unknown 2_8-P-helical structure.[38] MD simulation of this peptide in methanol starting from an extended structure and without any experimental restraints, viz. $V^{Q,\mathrm{restr}} = 0$, resulted in a structural ensemble dominated by the well-known 2.5_{12}-P-helix.[37] Since the set of 20 NMR model structures and the ensemble of MD generated trajectory structures showed virtually no overlap,[37] one might naively conclude that "the simulation did not match experiment". However, this would be incorrect. The ^3J-couplings and NOE distances calculated from the MD trajectories showed an average deviation of 0.44 Hz and two NOE bound violations of 0.05 nm. The 20 NMR model structures, which were derived using the NOE bounds, showed an average deviation of 0.57 Hz and, as expected, no NOE bound violations.

This example shows that derived quantities Q^{der} such as molecular structures should not be relied on to validate simulations. In particular, they should not be used in a restraining function $V^{Q,\mathrm{restr}}$. For some non-observable, derived quantities Q^{der} the assumptions and approximations involved in the procedure f relating Q^{der} to $\langle Q^{\mathrm{obs}} \rangle_{\mathrm{exp}}$ are of less importance than in the case sketched above. For example, in the absence of spin diffusion, NOE distance bounds

to r_{ij}^{-p} with $r_{ij} = |\vec{r}_i - \vec{r}_j|$ and $p = 3$ or 6, may represent the NOE intensities $I_{i,j}(\vec{r}^N)$ well. Another example are S^2 NMR order parameters, which are derived from spectra based on well defined assumptions. The S^2 order parameter is equal to the long-time plateau value of an auto-correlation function involving the vector connecting two nuclei. Thus S^2 values cannot be related to a single configuration $\vec{r}^N$, but only to an average, see Table 1. When using such derived quantities in a restraining function, one must make allowance for the uncertainty introduced into the $Q^{\rm der}$ values due to the procedure f.

2.2 Insufficient experimental data

If the number of items of experimental data on a given biomolecular system is lower than the number of its degrees of freedom, or if these items are correlated, it may not be possible to uniquely determine the conformation of a molecule that dominates the configurational ensemble. An example is the β-octa-peptide discussed in the previous section.[37] The 40 NOE distance bounds and 12 ^3J-couplings are insufficient to uniquely determine the dominant conformer. The set of 20 NMR model structures is distinct from the MD trajectory. While the latter is dominated by a 2.5_{12}-P-helix, the former corresponds to a 2_8-P-helix.[38] Other examples can be found in Refs. 39 and 40. The less independent experimental values of $Q^{\rm obs}$ that are available, the more the set or ensemble of structures derived from them will depend on the quality of the molecular model or force field $V^{\rm phys}(\vec{r}^N)$ used.

2.3 Accuracy of the (physical) force field

Of all the experimental techniques mentioned in the Introduction, high-resolution X-ray diffraction of crystals yields the highest information density. A protein may easily give rise to thousands or ten thousands of individual reflections. Due to this abundance of restraints in $V^{Q,\mathrm{restr}}$, the force field V^{phys} used in crystallographic structure refinement can be rather simple, e.g. containing only covalent bond-length, bond-angle and torsional-angle terms in conjunction with short-range (repulsive or van der Waals) interaction terms. The lack of long-range electrostatic and hydrogen-bonding interaction terms is assumed to be compensated by the large number of structure-factor amplitude restraints in $V^{Q,\mathrm{restr}}$. However, other experimental techniques have a much lower information density. This means inappropriate structures may be generated if an inadequate force field is used. This can again be illustrated by the case of the β-octa-peptide discussed in the previous sections. The use of a simple volume-based force field lacking electrostatic or hydrogen-bonding interaction terms in vacuo and the requirement that the experimental data be satisfied by a single-structure during the refinement procedure led to a 2_8-P-helix be proposed. This is despite the fact that such a helix had not been observed previously. In contrast the ensemble generated by MD simulation using a thermodynamically calibrated force field for this peptide in solution indicated the well-known 2.5_{12}-P-helix was dominant. Based on the performance of the latter force field regarding the reproduction of folding equilibria of peptides,[41, 42] the 2.5_{12}-P-helix is much more likely to represent reality than a 2_8-P-helix. The other experimental techniques mentioned in the Introduction have an even lower information density than NMR spectroscopy. This makes the quality of the molecular model or force field used

in the derivation of structure from such experimental data progressively more important and often the dominant factor.

2.4 Accuracy and consistency of the experimental data

In many cases the process of deriving structural information from experimental data will indicate that the experimental data contain inaccuracies or inconsistencies.[43] In the case of redundant experimental data, simulation techniques may be used to trace the source of these inconsistencies. An example is the investigation of 103 $^3J_{N-H\beta}$ and 94 $^3J_{H\alpha-H\beta}$ coupling data for the 107 residue FK506-binding protein FKBP.[43] The ^3J-couplings related to the χ_1 torsional angle of the residues. These were separated into χ_1 angles for which 0, 1, 2, 3 or 4 measured ^3J-couplings were available. Using Karplus relations to connect the χ_1-angle to the different ^3J-couplings, it was possible to examine whether there was a single χ_1-angle value that would reproduce, allowing for an uncertainty of 1 Hz in the Karplus relations, the different experimental ^3J-coupling values belonging to that torsional angle. No single χ_1-angle value could satisfy all the available data in 23 of the 63 residues.[43] Thus, a single-structure refinement procedure based on the ^3J-couplings for these 23 residues would result in erroneous χ_1-angle values. Because experimental ^3J-couplings are averages and the Karplus relation is non-linear in χ_1, averaging of the ^3J-couplings may lead to ranges of χ_1-angle values that are compatible with the observed ^3J-couplings: for 18 of the 23 residues such a range of χ_1-angle values could be found. However, for 5 of these χ_1-angles the only conclusions that could be drawn were that either one or more of the experimental ^3J-couplings for such a χ_1-angle must be incorrect or the use of the Karplus relation was inappropriate.[43]

So, if redundant experimental data are available for a particular degree of freedom or for a small set of degrees of freedom, these may be used to detect inconsistencies between different experimental data, which in turn hint at mistakes in the experiment, e.g. in the assignment of NOE signals to atom pairs or in the structures. We note, however, that experimental data $\langle Q \rangle_{\text{exp}}$ from different measurements may seem conflicting when they result from different time windows of sensitivity of the different measurements. In addition, compennsation of errors may occur. Unfortunately, most of the experimental techniques mentioned in the Introduction rarely yield redundant experimental data for a particular degree of freedom or a set of degrees of freedom of a system. Generally, indications that some or all of the experimental data may be problematic becomes evident when structures display a very high internal potential energy as a consequence of forcing the molecule to satisfy a set of inappropriate or conflicting restraints Q^{exp}, see Section 2.7.

2.5 Accuracy of the function $Q(\vec{r})$ relating observable Q to structure

The function $Q(\vec{r})$ that relates an observable quantity Q to a structure $\vec{r}$ even if postulated based on quantum-chemical theory or a set of physically reasonable assumptions will still involve approximations and rely on a given set of parameters and parameter values. For example, a ^3J-coupling can be related to a particular torsional angle θ through the Karplus relation (Table 1). The parameters a, b and c of the Karplus relation depend on the atoms involved in the ^3J-coupling and their covalently bound neighbours. These are normally calibrated using a set of measured ^3J-couplings thought to be associated with

particular θ-values in a given structure or molecular fragment. Figure 1 shows various parametrisations available in the literature. As can be seen, they lead to differences of up to 3 Hz for particular angles θ.[23, 43, 44] Although ^3J-couplings generally show a low experimental uncertainty, lower than 0.1 Hz, use of the Karplus relation may introduce an uncertainty of 1-2 Hz. Again allowance should be made for such uncertainties when using such data in structure determination.

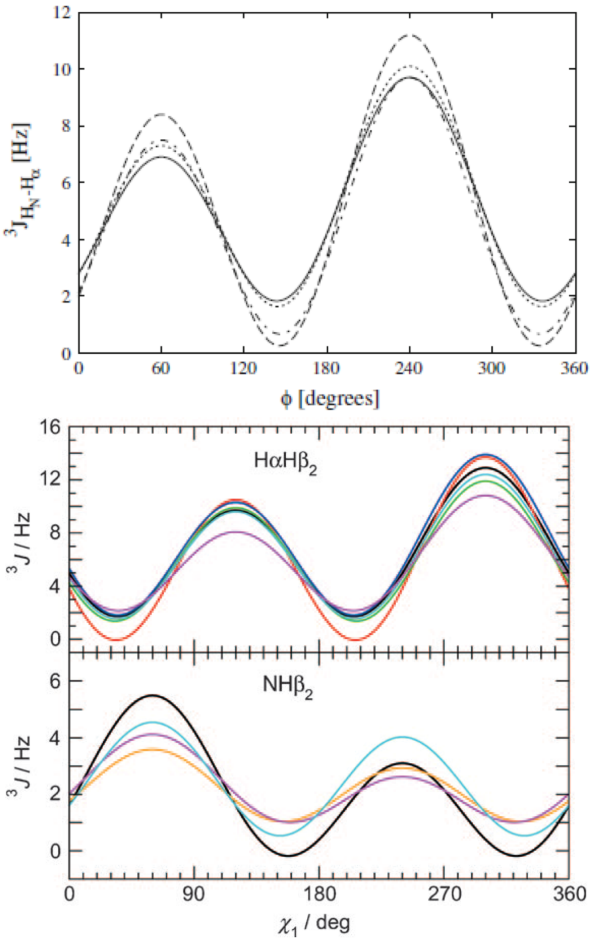

Figure 1: The variety of Karplus relations for the $^3J_{H_N H_\alpha}$- (upper panel), $^3J_{H_\alpha H_\beta}$-, and $^3J_{H_N H_\beta}$-coupling values (lower panels) describing the ^3J-coupling as function of the backbone ϕ-angle and side chain χ_1-angle of an amino acid. Upper panel:[44] The curves shown are from (solid line) Pardi et al.,[46] (dashed line) Brüschweiler and Case,[47] (dotted line) Wang and Bax,[48] and (dash-dotted line) Schmidt et al.[49] Lower panels:[43] The curves shown are from (black) DeMarco et al.,[50,51] (red) Abraham et al.,[52] (green) Deber et al.,[53] (blue) Cung et al.,[54] (cyan) Fischman et al.,[55] (magenta) Pérez et al.[56] (NMR-based parameterization), and (orange) Pérez et al.[56] (X-ray-based parameterization).

If different types of ^3J-couplings related to a particular torsional angle can be measured with high precision,[45] leading to a larger number of independent data points, it is possible to investigate the effect of varying (additional) model

parameters on the fit of ^3J-couplings calculated using the Karplus relation to measured ^3J-coupling values for a particular protein.[45] However, increasing the number of changeable parameters of a model may also mask the approximations and assumptions that affect the calculated ^3J-coupling values. By allowing variations in parameters of the function $Q(\vec{r})$, the force field used or the structures $\vec{r}^N$ used to calculate Q-values, the inability of a particular function $Q(\vec{r})$ to match all $Q^{\exp}$ values may be alleviated, but not eliminated.

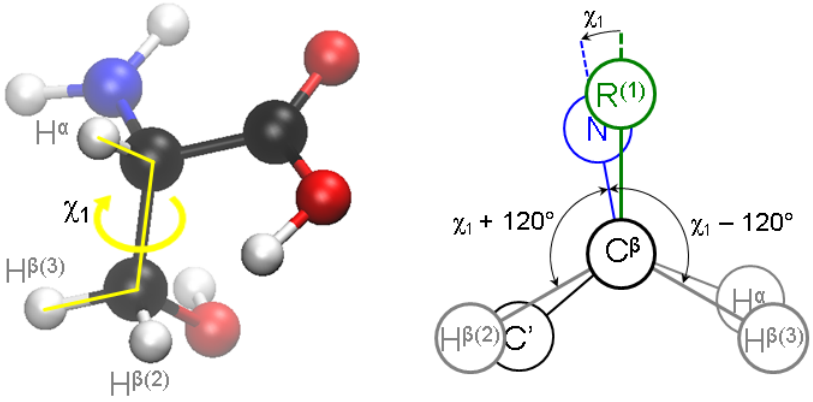

Figure 2: The relationship between the amino-acid side-chain torsional angle χ_1, the hydrogen atom H_α bound to the C_α atom and the hydrogen atoms $H_{\beta 2}$ and $H_{\beta 3}$ bound to the C_β atom. Nitrogen: blue; oxygen: red; carbon: black; hydrogen: grey; remaining atoms in side chain (R): green.

Other functions $Q(\vec{r})$ will also suffer from inaccuracy or uncertainty. When calculating NMR chemical shifts for a variety of MD trajectory structures of a β-hepta-peptide in solution using semi-empirical quantum-chemical theory, the chemical shifts obtained displayed little sensitivity to the underlying conformation compared to the variation due to different quantum-chemical approximations.[57] This can make the use of chemical shift values in structure refinement unreliable. Despite this chemical shift data in combination with empirical re-

lations between chemical shift and secondary structure is increasingly used in protein structure refinement.[58, 59]

Förster Resonance Energy Transfer (FRET) depends on the distance and relative orientation of the transition dipole vectors of a donor and an acceptor fluorophore. In most applications, isotropic orientational tumbling of the dipole vectors is assumed. This leads the FRET signal to be interpreted in terms of a single distance dependence. This greatly limits the accuracy of the distance distributions that are derived from measured FRET intensities.[15, 16]

2.6 Choice of the biasing function $V^{Q,\mathrm{rest}}(\vec{r}^N)$ to guide $\langle Q \rangle_{\mathrm{sim}}$ towards Q^{exp}

The goal of adding a biasing or restraining function $V^{Q,\mathrm{restr}}\left(Q(\vec{r}^N); Q^\circ\right)$ to the physical interaction function $V^{\mathrm{phys}}(\vec{r}^N)$ representing the molecular model is to keep the value of the quantity $Q(\vec{r}^N)$ close to the target value Q°, which is related to the experimentally observed value Q^{exp},

$$Q^\circ = Q^{\mathrm{exp}} + \Delta Q^{\mathrm{corr}}. \tag{6}$$

ΔQ^{corr} represents a correction to the Q^{exp} value that depends on the quantity Q and its relation to molecular structure (see below).

The functional form of $V^{Q,\mathrm{restr}}\left(Q; Q^\circ\right)$ should meet the following conditions (Figure 3).[60]

1. It should be a continuous function with a continuous derivative in order to obtain continuous energy and force in an MD simulation.

2. It should have two or three ranges that display a different behaviour of

399 the restraining force as function of Q.

400 (a) a flat-bottom region of zero restraining energy and zero restraining
401 force around Q°, e.g. for $[Q^\circ - \Delta Q^{\mathrm{fb}}, Q^\circ + \Delta Q^{\mathrm{fb}}]$.

402 (b) a region in which the restraining energy and force increase with in-
403 creasing deviation of Q from Q°, e.g. for $[Q^\circ \pm \Delta Q^{\mathrm{fb}}, Q^\circ \pm \Delta Q^{\mathrm{fb}} \pm$
404 $\Delta Q^{\mathrm{h}}]$.

405 (c) a region in which the restraining force reaches a constant maximum
406 in order to avoid too large restraining forces distorting the molecular
407 structure if the deviation of Q from Q° gets large, e.g. for $[Q^\circ \pm$
408 $\Delta Q^{\mathrm{fb}} \pm \Delta Q^{\mathrm{h}}, \pm\infty]$.

409 3. The restraining can be either purely attractive, that is apply when $Q > Q^\circ$,
410 e.g. as in the case of NOE atom-atom distance upper bound restrain-
411 ing,[30,31] purely repulsive, that is apply when $Q < Q^\circ$, e.g. when repre-
412 senting the absence of NOE intensity in a spectrum[61] or a combination
413 of attractive and repulsive restraining, e.g. as in the case of ^3J-coupling
414 restraining.[62]

The simplest representation of such a three-stage restraining function is a flat-bottom, then harmonic, then linear function

$$\begin{aligned} V^{Q,\mathrm{restr}}\left(Q; K^{Qr}, Q^\circ, \Delta Q^{\mathrm{fb}}, \Delta Q^{\mathrm{h}}\right) = {} & \frac{1}{2} K^{Qr} (Q - Q^\circ - \Delta Q^{\mathrm{fb}})^2 \\ & \cdot H(Q; Q^\circ + \Delta Q^{\mathrm{fb}}) \left[1 - H\left(Q; Q^\circ + \Delta Q^{\mathrm{fb}} + \Delta Q^{\mathrm{h}}\right)\right] \\ & + K^{Qr} \left(Q - Q^\circ - \Delta Q^{\mathrm{fb}} - \frac{1}{2}\Delta Q^{\mathrm{h}}\right) \Delta Q^{\mathrm{h}} \\ & \cdot H(Q; Q^\circ + \Delta Q^{\mathrm{fb}} + \Delta Q^{\mathrm{h}}) \cdot \\ \text{for } Q > Q^\circ \quad , & \end{aligned} \tag{7}$$

and

$$V^{Q,\mathrm{restr}}\left(Q; K^{Qr}, Q^{\circ}, \Delta Q^{\mathrm{fb}}, \Delta Q^{\mathrm{h}}\right) = \frac{1}{2} K^{Qr} (Q - Q^{\circ} + \Delta Q^{\mathrm{fb}})^2 \cdot \left[1 - H(Q; Q^{\circ} - \Delta Q^{\mathrm{fb}})\right] H(Q; Q^{\circ} - \Delta Q^{\mathrm{fb}} - \Delta Q^{\mathrm{h}}) - K^{Qr} \left(Q - Q^{\circ} + \Delta Q^{\mathrm{fb}} + \frac{1}{2} \Delta Q^{\mathrm{h}}\right) \Delta Q^{\mathrm{h}} \cdot \left[1 - H\left(Q; Q^{\circ} - \Delta Q^{\mathrm{fb}} - \Delta Q^{\mathrm{h}}\right)\right] \quad \text{for } Q < Q^{\circ}, \tag{8}$$

where $\Delta Q^{\mathrm{fb}} \geq 0$ and $\Delta Q^{\mathrm{h}} \geq 0$, and the Heaviside step function $H(x; x_0)$ is defined by

$$\begin{aligned} H(x; x_0) &= 0 \quad \text{for } x < x_0 \\ &= 1 \quad \text{for } x \geq x_0 \,. \end{aligned} \tag{9}$$

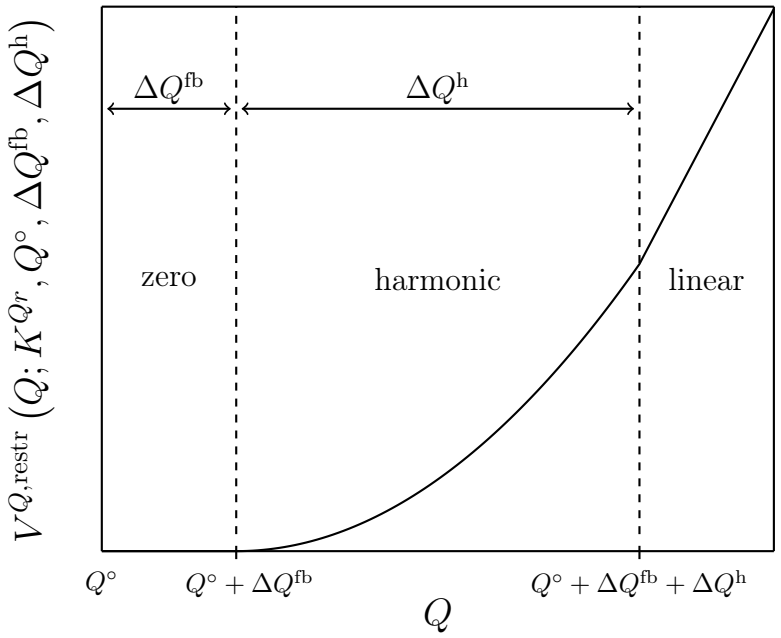

Figure 3: Potential energy term $V^{Q,\mathrm{restr}}\left(Q; K^{Qr}, Q^\circ, \Delta Q^{\mathrm{fb}}, \Delta Q^{\mathrm{h}}\right)$ for restraining the quantity Q.[60]

The corresponding force along Q, i.e. the negative of the derivative of $V^{Q,\mathrm{restr}}$ with respect to Q is then for $Q > Q^\circ$,

$$
\begin{aligned}
f^{Q,\mathrm{restr}} &= 0 && \text{for} \quad Q < Q^\circ + \Delta Q^{\mathrm{fb}} \\
&= -K^{Qr}\left(Q - Q^\circ - \Delta Q^{\mathrm{fb}}\right) && \text{for} \quad Q^\circ + \Delta Q^{\mathrm{fb}} \leq Q \leq Q^\circ + \Delta Q^{\mathrm{fb}} + \Delta Q^{\mathrm{h}} \\
&= -K^{Qr}\Delta Q^{\mathrm{h}} && \text{for} \quad Q > Q^\circ + \Delta Q^{\mathrm{fb}} + \Delta Q^{\mathrm{h}}, \qquad (10)
\end{aligned}
$$

and for $Q < Q^\circ$,

$$
\begin{aligned}
f^{Q,\mathrm{restr}} &= 0 && \text{for} \quad Q > Q^\circ - \Delta Q^{\mathrm{fb}} \\
&= -K^{Qr}\left(Q - Q^\circ + \Delta Q^{\mathrm{fb}}\right) && \text{for} \quad Q^\circ - \Delta Q^{\mathrm{fb}} - \Delta Q^{\mathrm{h}} \leq Q \leq Q^\circ - \Delta Q^{\mathrm{fb}} \\
&= +K^{Qr}\Delta Q^{\mathrm{h}} && \text{for} \quad Q < Q^\circ - \Delta Q^{\mathrm{fb}} - \Delta Q^{\mathrm{h}}\,. \qquad (11)
\end{aligned}
$$

To obtain the force on particle i, these expressions are multiplied by ${}^{\partial Q(\vec{r}^N)}/_{\partial \vec{r}_i}$, the derivative of Q with respect to $\vec{r}_i$. Of course, other functional forms of the restraining function that match the basic requirements, such as a Gaussian form, may be used.

In certain NMR experiments, the signals from different hydrogen atoms may not be distinguishable, e.g. for the three hydrogen atoms of a CH_3 group. In such a case the (distance) restraint is applied to a so-called pseudo-atom position.[63] Such a position is defined in terms of the positions of the hydrogen atoms and the atoms these are bound to, see Figure 4. The use of pseudo atoms in the restraining requires corrections ΔQ^{corr} to the distance bounds Q^{exp} derived from experiment.[60, 63–65] Figure 4 shows three sets of ΔQ^{corr} values for NOE distance bounds that are used in structure determination based on NOE data. An alternative is to use so-called ambiguous restraints, in which the sum of the $r^{-1/6}$ weighted distances to the different indistinguishable hydrogens is used in the restraining function.[66, 67]

Geometry	Wüthrich (1983) correction (nm)	Fletcher (1996) correction (nm)	GROMOS (1996) correction (nm)
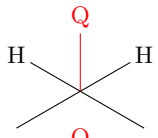	+0.10	+0.07	+0.09
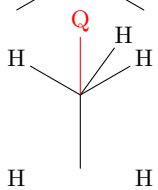	+0.15	+0.04	+0.10
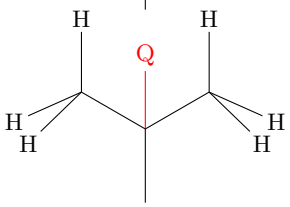	+0.29	+0.15	+0.22
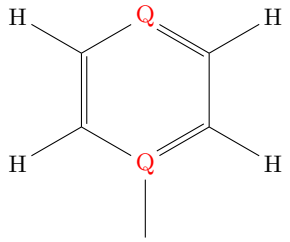	+0.20	+0.20	+0.21

Figure 4: Geometries and NOE distance bound corrections for pseudo atoms Q, from Wüthrich et al.,[63] Fletcher et al.,[65] and van Gunsteren et al., GROMOS..[64] Fletcher et. al.[65] also apply a multiplicity correction when an NOE signal is known to arise from an averaging over several hydrogens. For an NOE between groups of hydrogen atoms A and B, the upper bound is then scaled by a factor $(n_A n_B)^{\frac{1}{p}}$, where p corresponds to the power (3 or 6) of the distance averaging and n_A and n_B are the number of equivalent hydrogen atoms in each group.

2.7 Weight of the restraining function $V^{Q,\text{restr}}$ relative to that of the force field energy V^{phys}

The relative weight of the biasing or restraining term $V^{Q,\text{restr}}$ compared to that of the physical force field term V^{phys} in the total potential energy (Eq. 4) of the system is determined by the size of the force constant K^{Qr} in $V^{Q,\text{restr}}$.

The larger the weight or K^{Qr}, the smaller will be the deviation of Q from Q°. However, if the agreement with the experimental data is forced excessively this will result in a higher V^{phys} of the system or a higher internal energy of the molecule to which the restraints are applied. The molecule will simply adopt a more strained conformation in order to match the values Q°.

An early example and analysis of the effect of restraining too strongly can be found in Ref. 68. While deriving a spatial structure of the headpiece of the protein lac repressor, two structures were obtained, structure I in which a loop was incorrectly folded (total NOE bounds violation: 3.242 nm), and structure II in which the loop was correct (total NOE bounds violation: 0.405 nm).[61] The structure refinement procedure was based on MD simulation followed by energy minimization (EM) in the presence of 215 attractive NOE atom-atom distance restraints with $K^{Qr} = 17 \cdot 10^3$ kJ mol^{-1} nm^{-2}, then followed by EM, 5 ps of MD and again MD simulation with $K^{Qr} = 0$.[68] The results in Table 2 show that MD refinement with a large weight, $K^{Qr} = 17 \cdot 10^3$ kJ mol^{-1} nm^{-2}, results in the incorrect structure having lower NOE bound violations, 0.180 nm, than the correct structure, 0.258 nm. However, this results in a higher intra-protein potential energy, -2996 kJ mol^{-1} compared to -3053 kJ mol^{-1}. When the restraining term $V^{Q,\mathrm{restr}}$ is switched off, $K^{Qr} = 0$, the molecule relaxes resulting in much larger NOE bound violations for the structure containing the wrongly folded loop. This example illustrates that molecular structures derived from experimental data should not only match that data, but must also have a low energy. Otherwise one may satisfy the experimental data but obtain a strained, unstable conformation.

Table 2: MD refinement of lac repressor structures.[68] A set of 215 NOE distance bounds for pairs of atoms were used in the half-harmonic attractive restraining term of the potential energy function with a weight K^{Qr}. The GROMOS biomolecular force field[76,77] was used as interaction function. The two initial structures I and II of the protein were taken from Ref. 61.

		Structure I Loop wrongly folded			Structure II Loop correctly folded		
	K^{Qr} (kJ mol^{-1} nm^{-2})	constraint violation (nm)		energy (kJ mol^{-1})	constraint violation (nm)		energy (kJ mol^{-1})
		sum	average		sum	average	
Initial structure		3.242	0.015	-2115	0.405	0.002	-3092
After 5 ps MD + EM	17000	0.180	0.001	-2996	0.258	0.001	-3053
After EM	0	0.523	0.002	-3083	0.461	0.002	-3100
After 5 ps MD + EM	0	3.297	0.015	-3032	1.823	0.008	-3102

This leads to the question how low should be the energy of a molecule. This depends on the force field used as V^{phys} and on the size and composition of the molecule. Table 3 presents the intra-protein potential energies of a number of proteins for which a high-resolution X-ray crystal structure is available and for some proteins the structures of which have been derived on the basis of NMR NOE atom-atom distance bounds.[68] The NOE bound based structures of the lac repressor and of tendamistat both have energies comparable to those of X-ray diffraction based structures of proteins of similar size. In contrast, the last five structures in Table 3 display a relatively high energy, at least about 1000 kJ mol^{-1} higher than an X-ray structure of comparable size. This is most likely due to the use of a large value for the restraining force constant K^{Qr}, which lowers the distance bound violations at the expense of a high internal energy. The discrepancy in energy cannot be due to the application of different force fields. The biomolecular force fields used, CHARMM[78] and GROMOS,[76,77] consist of comparable interaction terms: while the CHARMM force field yields an energy of -2247 kJ mol^{-1} for the crambin X-ray structure, the GROMOS force field yields a comparable value of -2161 kJ mol^{-1}. The structures of the last five proteins in Table 3 are likely to be highly strained.

This example illustrates that reporting and depositing structures of doubtful quality is not a new phenomenon. It is a consequence of the understandable tendency of researchers to push experimental and theoretical methods to the limit of what they can do. Currently many structures of large protein assemblies are being determined using electron microscopy and then used as initial structures for MD simulations. Here it is likely that similar problems as in the example given will be found in some of these structures. This state of affairs calls for a

continuous effort of the scientific community towards validation of structures in data bases[79–81] and if needed their improvement.[81]

In this regard it is of interest to track the fate of the highly strained structures discussed above in Table 3. None of the structures reported in Refs. 71–75 are currently available in the PDB. So they were either never deposited or removed. The structure of hirudim[71] was deposited in 1990 and has been updated multiple times, the latest in 2009.

If different sets of experimental data, such as NOEs, RDCs, ^3J-couplings or X-ray structure factor amplitudes are used simultaneously when restraining, there is a need to provide the relative weights of the different sets of Q^{exp} values originating from different experiments.[82] However, it is not possible to do this in an objective fashion.

Table 3: Energies of X-ray and NMR protein structures.[68] N_{Qr}: number of distance restraints. K^{Qr}: weight of the restraining function. The GROMOS[76,77] or the CHARMM[78] biomolecular force field was used as interaction function. For tendamistat the highest and lowest energy for a set of structures is given.

	Number of residues	Source of data or structure	N_{Qr}	K^{Qr} (kJ mol^{-1} nm^{-2})	Average violation (nm)	Protein energy (kJ mol^{-1})	Force field used
aPP	36	X-ray[35]				-2180	GROMOS
crambin	46	X-ray[35]				-2161	GROMOS
BPTI	58	X-ray[35]				-3529	GROMOS
Phospholipase A2	123	X-ray[35]				-7848	GROMOS
Lac repressor	51	NMR[61]	215	4000	0.003	-3091	GROMOS
tendamistat	74	NMR[69]	842			-3140	GROMOS
						-2834	GROMOS
crambin	46	X-ray/NMR[70]	240	5000	0.033	-2247	CHARMM
hirudin	56	NMR[71]	359	17000	0.016	-1138	CHARMM
Histone H5	79	NMR[72]	307	17000	0.015	-1527	CHARMM
CPI	39	NMR[73]	309	33000	0.007	-724	CHARMM
phoratoxin	46	NMR[74]	331	33000	0.010	-1029	CHARMM
A1-purothionin	46	NMR[75]	310	33000	0.023	-498	CHARMM

2.8 Averaging over space and time

Values of $Q^{\exp}$ of experimentally measured properties correspond in general to averages of a quantity Q over both space (or molecules) and time,

$$Q^{\exp} = \left\langle \langle Q \rangle_{\text{space}} \right\rangle_{\text{time}} \quad , \tag{12}$$

where the angular brackets denote averaging (Eq. 2) over the distribution $P(\vec{r}^N)$ of configurations of the system, e.g. the Boltzmann distribution (Eq. 1).

Time averaging when restraining was first introduced[83] in relation to the use of NOE derived atom-atom (i, j) distance, r_{ij}, information with $Q = r_{ij}^{-3}$ or $Q = r_{ij}^{-6}$. This was later followed by application to crystallographic structure factor amplitude restraining,[84–87] chemical shift restraining,[58] ^3J-coupling restraining[62, 88] and S^2 NMR order parameter restraining.[89] Time-averaging restraining methods are characterized by two parameters, the force constant or weight K^{Qr} of the restraining function $V^{Q,\text{restr}}$ and the memory relaxation time τ_Q representing the time span over which $Q(\vec{r}^N(t))$ is to be averaged. The time-averaged value of Q is commmonly exponentially damped

$$\left\langle Q(\vec{r}^N) \right\rangle_t = \left[\tau_Q \left(1 - \exp(-t/\tau_Q)\right)\right]^{-1} \int_0^t \exp(-(t-t')/\tau_Q) Q(\vec{r}^{\,N}(t'))\mathrm{d}t', \tag{13}$$

in the restraining function $V^{Q,\text{restr}}$ (Eqs. 7 and 8) in order to avoid that the restraining force progressively approaches zero with time.[83] Time-averaging restraining has been investigated as function of K^{Qr} and τ_Q for a variety of systems.[44, 83–96] The force constant K^{Qr} should be taken as small as possible in order to avoid a restraining bias that puts strain into the molecule, as discussed

in the previous section, while being large enough to force $\langle Q \rangle_{\mathrm{time}}$ to be close to Q°. In addition, too strong restraints may destroy the proper Boltzmann weighting (Eq. 1) of configurations of the trajectory. The memory relaxation time should be of the order of the experimental averaging time that determines Q^{exp}, but at least an order of magnitude shorter than the length of the MD simulation in order to secure sufficient statistics when averaging $Q\left(\vec{r}^{N}(t)\right)$ over t. In addition, the heating of the system due to the non-conservative force resulting from the time-averaging restraining term should be small.

The averaging over molecules can be accounted for by simulating N_m independent systems in parallel for which the initial coordinates and momenta $\left(\vec{r}^{N}(t_0), \vec{p}^{N}(t_0)\right)$ are Boltzmann-distributed in regard to V^{phys}. This is easily achieved in the case of the momenta $\vec{p}^{N}$, because the kinetic energy term in the Hamiltonian of the system is – in the absence of constraints – quadratic in the momenta, but rather difficult if not impossible for configurations $\vec{r}^{N}$ of a biomolecular system, because the potential energy term of the Hamiltonian is generally a complex function of the coordinates $\vec{r}^{N}$.[97] Relaxation times of biomolecular systems generally exceed the time scale accessible using MD simulation which means that if the initial configurations $\vec{r}^{N}(t_0)$ of the N_m systems are not Boltzmann distributed, the averages $\langle Q \rangle$ over the N_m systems are very likely to reflect non-Boltzmann averaging. Molecule-averaging restraints were again first introduced in relation to NOE-derived atom-atom distance information.[98, 99] Here, the molecule-averaged value of Q,

$$\left\langle Q(\vec{r}^{N}) \right\rangle_{\mathrm{molecules}} = \sum_{n=1}^{N_m} p_n Q(\vec{r}_n^{N}), \tag{14}$$

with

$$p_n = N_m^{-1}, \tag{15}$$

or

$$p_n = \frac{\exp\left(-V^{\mathrm{phys}}(\vec{r}_n^N)/(k_\mathrm{B}T)\right)}{\sum_{n'=1}^{N_m} \exp\left(-V^{\mathrm{phys}}(\vec{r}_{n'}^N)/(k_\mathrm{B}T)\right)}, \tag{16}$$

is used, instead of the single molecule value $Q(\vec{r}^N)$, in the restraining function $V^{Q,\mathrm{restr}}$ (Eqs. 7 and 8).[99] Molecule-averaging restraining methods are also characterized by two parameters, the force constant or weight K^{Qr} of the restraining function $V^{Q,\mathrm{restr}}$ and the number of molecules or systems N_m over which the averaging is performed.[100,101] However, problems can arise if the initial configurations $\vec{r}^N(t_0)$ are not Boltzmann distributed over the N_m systems and are given equal weight (Eq. 15) in the average $\langle Q \rangle$ (Eq. 14) unless the simulation is much longer than the system relaxation time. In such cases the average $\langle Q \rangle_{\mathrm{molecules}}$ will only be Boltzmann weighted in the limit of a large number of molecules N_m being used in combination with large restraining force constants K^{Qr},[102–104] and in the absence of noise in the target values Q°.[105] Unfortunately, neither condition is normally met in practice: (*i*) The number of systems N_m is generally kept low, i.e. 10-100, in order to minimize the computational effort; (*ii*) the force constant of the restraining function should be as small as possible, as discussed in the previous section; (*iii*) the experimental data Q^{exp} and the function $Q(\vec{r})$ relating Q to structure are generally not error free.

The problem of non-Boltzmann averaging over molecules may be alleviated by applying Hamiltonian replica-exchange techniques[106–108] that swap configurations between the N_m molecules or systems based on the Boltzmann proba-

bility of the respective configurations.[109, 110]

Since most structures of proteins deposited in the protein data bank were determined by single-structure refinement, i.e. not accounting for averaging, one may ask whether accounting for averaging in restraining is important. Unless the configurational ensemble of a molecule is very narrow and centered on a single dominant structure, the average over a Boltzmann distribution (Eq. 2) of structures $\vec{r}^N$, $\langle Q \rangle_{\vec{r}^N}$, will generally not be equal to the value of Q calculated for a single structure $\vec{r}^N$

$$\langle Q \rangle_{\vec{r}^N} \neq Q\left(\vec{r}^N\right), \tag{17}$$

and it will also not be equal to the value of Q calculated for the mean structure $\left\langle \vec{r}^N \right\rangle$,

$$\langle Q \rangle_{\vec{r}^N} \neq Q\left(\left\langle \vec{r}^N \right\rangle\right). \tag{18}$$

This is due to the non-linearity of the function $Q(\vec{r}^N)$ with respect to configurations $\vec{r}^N$ or the non-linearity of the Boltzmann weighting in Eq. 2. As a consequence, single-structure refinement, i.e. not accounting for averaging, may lead to highly distorted structures. An example can be found in Figure 5.[111] The NOE atom-atom distance bounds derived from NMR experiments on a β-hexa-peptide in methanol turned out to belong to two rather different conformations, a left-handed 3_{14} helix and right-handed $2.7_{10/12}$ helix which are both populated in solution. While single-structure refinement led to a distorted and strained structure (Figure 5, middle), MD simulation without any restraints sampled both helices and as a consequence satisfied all NOE bounds.[111] For proteins, accounting for averaging is particularly important in regard to the mobility of side chains. Single-structure refinement of the protein tendamistat

based on NOE data resulted in the side chain of 15 Tyr being placed in a single conformation that resulted in small NOE bound violations to spatially adjacent side chains. However, in the structure determined crystallographically of this protein no electron density was observed for the side chain of 15 Tyr, indicating it was highly mobile. This illustrates how single-structure refinement can lead to the underestimation of the structural variability within a molecule.[112, 113] This applies to X-ray crystallographic single-structure refinement as well as to that based on NMR.[86, 87]

Figure 5: Left: Molecular model for a β-heptapeptide derived from NMR data obtained in methanol. Left-handed 3_{14}-helix with hydrogen bonds: NH(i) — O($i+2$).[114] Middle: Molecular model for a β-hexapeptide derived using single-structure refinement using 34 distance restraints derived from NOE NMR data obtained in methanol. Average structure: Right-handed helix in MeOH with only one hydrogen bond: NH(4) — O(1). Distorted, due to 3 NOEs characteristic for a left-handed 3_{14}-helix.[115] Right: Molecular model for this β-hexapeptide derived from NMR data obtained in pyridine. Right-handed helix with hydrogen bonds: NH(i) — O($i+1, i-3$).[116] Hydrogen bonds (with a maximum proton - acceptor distance of 0.25 nm and a minimum donor-proton-acceptor angle of 135°) are shown with red dashed lines.

When applied to ^3J-coupling restraining, the use of the time-average $\langle Q \rangle_t$ (Eq. 13) in the quadratic part of the restraining function $V^{Q,\mathrm{restr}}$ (Eqs. 7, 8) led to large structural fluctuations.[96] This is due to the fact that the average $\langle Q \rangle_t$ of Q can lag behind the instantaneous value of $Q(t)$ of Q. If the restraining

force only depends on $\langle Q \rangle_t$, it may drive $Q(t)$ away from Q° in case $\langle Q \rangle_t$ and $Q(t)$ are at different sides of Q°. This effect was not observed in time-averaging NOE distance bound restraining because (*i*) only attractive distance restraints are used, (*ii*) the r^{-3} or r^{-6} distance dependence of the NOE signal gives most weight to short distances when averaging thereby reducing the difference between $Q(t)$ and $\langle Q \rangle_t$ for short distances $Q(t)$, and (*iii*) the van der Waals repulsion between atoms in V^{phys} prevents very small atom-atom distances $Q(t)$ being sampled.

The problem of $\langle Q \rangle_t$ lagging behind $Q(t)$ can be solved by using a biquadratic restraining function $V^{Q,\mathrm{restr}}$ that depends on both $Q(t)$ and $\langle Q \rangle_t$,[88]

$$\begin{aligned} V_{\mathrm{att}}^{Q,\mathrm{restr}}\left(Q(t), \langle Q \rangle_t ; K^{Qr}, Q^\circ, \Delta Q^{\mathrm{fb}}\right) = \frac{1}{2} K^{Qr} (Q(t) - Q^\circ - \Delta Q^{\mathrm{fb}})^2 \\ \cdot H\left(Q(t); Q^\circ + \Delta Q^{\mathrm{fb}}\right) \left(\langle Q \rangle_t - Q^\circ - \Delta Q^{\mathrm{fb}}\right)^2 \\ \cdot H\left(\langle Q \rangle_t ; Q^\circ + \Delta Q^{\mathrm{fb}}\right), \end{aligned} \tag{19}$$

for $Q(t) > Q^\circ$ and $\langle Q \rangle_t > Q^\circ$

$$\begin{aligned} V_{\mathrm{rep}}^{Q,\mathrm{restr}}\left(Q(t), \langle Q \rangle_t ; K^{Qr}, Q^\circ, \Delta Q^{\mathrm{fb}}\right) = \frac{1}{2} K^{Qr} (Q(t) - Q^\circ + \Delta Q^{\mathrm{fb}})^2 \\ \cdot \left[1 - H\left(Q(t); Q^\circ - \Delta Q^{\mathrm{fb}}\right)\right] \left(\langle Q \rangle_t - Q^\circ + \Delta Q^{\mathrm{fb}}\right)^2 \\ \cdot \left[1 - H\left(\langle Q \rangle_t ; Q^\circ - \Delta Q^{\mathrm{fb}}\right)\right], \end{aligned} \tag{20}$$

for $Q(t) < Q^\circ$ and $\langle Q \rangle_t < Q^\circ$. The corresponding force along Q, i.e. the negative of the derivative of $V^{Q,\mathrm{restr}}$ with respect to Q, is then for the case

$Q(t) > Q^\circ$ and $\langle Q \rangle_t > Q^\circ$,

$$
\begin{aligned}
f^{Q,\mathrm{restr}} &= 0 && \text{for} \quad Q(t) < Q^\circ + \Delta Q^{\mathrm{fb}} \text{ or } \langle Q \rangle_t < Q^\circ + \Delta Q^{\mathrm{fb}} \\
&= -K^{Qr} \Big\{ \left(Q(t) - Q^\circ - \Delta Q^{\mathrm{fb}} \right) \left(\langle Q \rangle_t - Q^\circ - \Delta Q^{\mathrm{fb}} \right)^2 \\
&+ \left(Q(t) - Q^\circ - \Delta Q^{\mathrm{fb}} \right)^2 \left(\langle Q \rangle_t - Q^\circ - \Delta Q^{\mathrm{fb}} \right) \cdot \left(1 - \exp\left(-\Delta t / \tau_Q \right) \right) \Big\} \\
& && \text{for} \quad Q(t) > Q^\circ + \Delta Q^{\mathrm{fb}} \text{ and } \langle Q \rangle_t > Q^\circ + \Delta Q^{\mathrm{fb}},
\end{aligned}
\tag{21}
$$

where the derivative of the average $\langle Q \rangle_t$ (Eq. 13) with respect to $Q(t)$ has been expressed in terms of discrete MD time steps Δt,

$$
\frac{\partial \langle Q \rangle_t}{\partial Q(t)} = \left(1 - \exp(-\Delta t / \tau_Q) \right). \tag{22}
$$

For the case $Q(t) < Q^\circ$ and $\langle Q \rangle_t < Q^\circ$ we have

$$
\begin{aligned}
f^{Q,\mathrm{restr}} &= 0 && \text{for} \quad Q(t) > Q^\circ - \Delta Q^{\mathrm{fb}} \text{ or } \langle Q \rangle_t > Q^\circ - \Delta Q^{\mathrm{fb}} \\
&= -K^{Qr} \Big\{ \left(Q(t) - Q^\circ + \Delta Q^{\mathrm{fb}} \right) \left(\langle Q \rangle_t - Q^\circ + \Delta Q^{\mathrm{fb}} \right)^2 \\
&+ \left(Q(t) - Q^\circ + \Delta Q^{\mathrm{fb}} \right)^2 \left(\langle Q \rangle_t - Q^\circ + \Delta Q^{\mathrm{fb}} \right) \cdot \left(1 - \exp\left(-\Delta t / \tau_Q \right) \right) \Big\} \\
& && \text{for} \quad Q(t) < Q^\circ - \Delta Q^{\mathrm{fb}} \text{ and } \langle Q \rangle_t < Q^\circ - \Delta Q^{\mathrm{fb}}.
\end{aligned}
\tag{23}
$$

To obtain the force on particle i, these expressions must be multiplied by ${\partial Q(\vec{r}^N(t))}/{\partial \vec{r}_i(t)}$. Using this biquadratic form, the restraining function only generates a force when both the instantaneous value $Q(t)$ of Q and the time-averaged value $\langle Q \rangle_t$ of Q lie outside the flat bottom of the restraining function $V^{Q,\mathrm{restr}}$.

If both, attractive ($Q > Q^\circ$) and repulsive ($Q < Q^\circ$) restraints are applied, the restraining is harmonic with a flat bottom. If $Q(t)$ and $\langle Q \rangle_t$ both lie outside the flat bottom and on the same side of Q°, the two terms in Eqs. 21 and 23 originating from the derivatives of $Q(t)$ and $\langle Q \rangle_t$ yield contributions to the force $f^{Q,\mathrm{restr}}$ that drive $Q(t)$ towards Q°. If $Q(t)$ and $\langle Q \rangle_t$ lie on different sides of Q°, i.e. $Q(t) < Q^\circ - \Delta Q^{\mathrm{fb}}$ and $\langle Q \rangle_t > Q^\circ + \Delta Q^{\mathrm{fb}}$ or $Q(t) > Q^\circ + \Delta Q^{\mathrm{fb}}$ and $\langle Q \rangle_t < Q^\circ - \Delta Q^{\mathrm{fb}}$, no restraining force is generated.

2.9 How to deal with a multiple-valued relation between structure and restrained quantity Q ?

For some of the quantities Q listed in Table 1, there is more than one configuration $\vec{r}^N$ that corresponds to the same Q value. An example of such a function $Q(\vec{r}^N)$ is the Karplus relation ${}^3J(\theta)$ that relates a ${}^3J$-coupling to a torsional angle θ, see Figure 1. There are up to four values of the angle θ that may correspond to a single ${}^3J$-coupling value. This implies that the inverse of ${}^3J(\theta)$, the function $\theta({}^3J)$, is multiple-valued. Depending on the initial value of the angle θ, the restraining function $V^{Q,\mathrm{restr}}$ may drive the angle θ in different directions to one of the different angle values that correspond to ${}^3J^\circ$. This is illustrated in the upper panels of Figure 6. If the target ${}^3J^\circ$-value lies beyond one maximum or minimum of the function ${}^3J(\theta)$, but not beyond another maximum or minimum, the restraining function $V^{Q,\mathrm{restr}}$ may drive the angle θ in the wrong direction. This is illustrated in the lower right panel of Figure 6. Thus if the function $\vec{r}^N(Q)$ is multiple-valued, the restraining techniques discussed so far may not lead to structures that match the target Q° values. This problem can be solved by driving the structure out of the range of θ-values for which $V^{Q,\mathrm{restr}}$

has a low energy but where these energies cannot become zero.

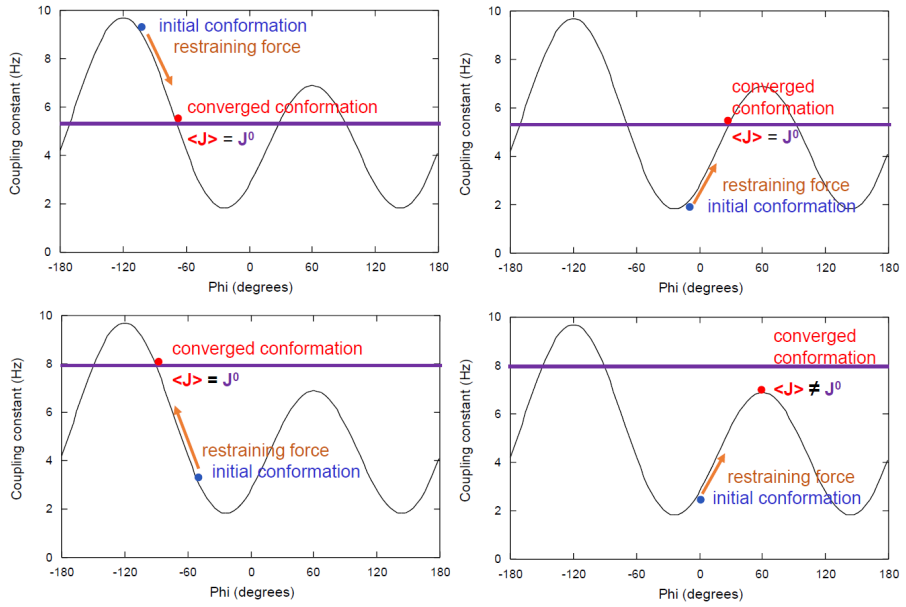

Figure 6: Consequences of a multiple-valued function $\phi(^3J)$ for restraining an angle ϕ to a particular ^3J-coupling value J° when starting from different initial values of ϕ in structure refinement.

A technique that achieves this, local-elevation sampling, has been proposed more than two decades ago.[117] It adds a memory function $V^{\mathrm{le}}(\phi^M)$ depending on a set $\phi^M \equiv (\phi_1, \phi_2, \ldots, \phi_M)$ of torsional or dihedral angles ϕ_k defined by four atoms or particles $(k_1 - k_2 - k_3 - k_4)$ to the physical interaction function V^{phys}. This memory function can have the form of a Gaussian of width $\Delta\phi^\circ$ centered at the value ϕ_i°. For a given torsional angle ϕ_k, $V_k^{\mathrm{le}}(\phi_k)$ is a sum of N_{le} Gaussians centered at generally equidistant values ϕ_i°, which are the same for each k, with $i = 1, 2, \ldots, N_{\mathrm{le}}$ along the 360° range of ϕ_k values,

$$V_k^{\mathrm{le}}\left(\phi_k(t)\right) = \sum_{i=1}^{N_{\mathrm{le}}} V_k^{\mathrm{le}}\left(\phi_k(t); \phi_i^\circ\right), \tag{24}$$

with

$$V_k^{\mathrm{le}}\left(\phi_k(t);\phi_i^\circ\right) = K^{\mathrm{le}}\omega\left(\phi_k(t);\phi_i^\circ\right)\exp\left(-\frac{\left(-\phi_k(t)-\phi_i^\circ\right)^2}{2\left(\Delta\phi^\circ\right)^2}\right). \tag{25}$$

K^{le} is the overall weight of the local-elevation contribution to the potential energy, while the weight factor $\omega\left(\phi_k(t);\phi_i^\circ\right)$ is enlarged by a given amount $\Delta\omega$ at every time point t for which

$$\phi_i^\circ - \frac{1}{2}\Delta\phi^\circ \leq \phi_k(t) \leq \phi_i^\circ + \frac{1}{2}\Delta\phi^\circ. \tag{26}$$

In this way the total potential energy surface for the molecular configuration at the point defined by the local-elevation variables, i.e. torsional angles ϕ^M, i.c. at position ϕ_i°, is lifted or locally elevated every time the molecule visits the region around ϕ_i° during the MD simulation. In this way the system is driven away from regions of configurational space that were visited previously. Multiple equivalent schemes have been proposed. For example, in 2002 the local-elevation sampling technique was republished under the name "metadynamics".[118]

The local-elevation sampling technique can also be used when restraining structure $\vec{r}^N$ or θ towards Q° or ${}^3J^\circ$ values when the function $\vec{r}^N(Q)$ or $\theta({}^3J)$ is multiple-valued.[119] In this case the local-elevation function V_k^{le} of Eqs. 24 and 25 is used as biasing or restraining function $V^{Q,\mathrm{restr}}$, but the way the weight $\omega\left(\phi_k(t);\phi_i^\circ\right)$ in Eq. 25 is assigned is varied. The weight is only increased when both $Q(t)$ and $\langle Q\rangle_t$ lie outside the flat bottom of $V^{Q,\mathrm{restr}}$. With $Q = {}^3J_k$ we have, using a biquadratic attractive ($Q(t) > Q^\circ$ and $\langle Q\rangle_t > Q^\circ$) and repulsive ($Q(t) < Q^\circ$ and $\langle Q\rangle_t < Q^\circ$) flat-bottom function of $Q(t)$ and $\langle Q\rangle_t$,

$$\omega\left(\phi_k(t);\phi_i^\circ\right) = t^{-1}\int_0^t \delta_{\phi_k(t')\phi_i^\circ} \cdot\Big\{V_{\text{att}}^{Q,\text{restr}}\left(Q(t'),\langle Q\rangle_{t'};K^{Qr},Q^\circ,\Delta Q^{\text{fb}}\right) + V_{\text{rep}}^{Q,\text{restr}}\left(Q(t'),\langle Q\rangle_{t'};K^{Qr},Q^\circ,\Delta Q^{\text{fb}}\right)\Big\}\mathrm{d}t', \tag{27}$$

with

$$\delta_{\phi_k(t)\phi_i^\circ} = \begin{cases} 1 & \text{if } \phi_i^\circ - \dfrac{\Delta\phi^\circ}{2} \le \phi_k(t) \le \phi_i^\circ + \dfrac{\Delta\phi^\circ}{2} \\ 0 & \text{otherwise} \end{cases} . \tag{28}$$

This local-elevation biasing technique has been shown to generate structural ensembles that match the Q^{exp} data used in the biasing function.[44, 120, 121]

Local-elevation biasing of a MD simulation based on target Q° values of a quantity Q can also be used to detect inconsistencies between different experimental Q^{exp} values.[43] This is illustrated in Figure 7 for the case of four ^3J-coupling values, $^3J_{H_\alpha H_{\beta 2}}$ (4.0 Hz), $^3J_{H_\alpha H_{\beta 3}}$ (2.0 Hz), $^3J_{NH_{\beta 2}}$ (1.8 Hz), $^3J_{NH_{\beta 3}}$ (1.8 Hz) belonging to one torsional angle $\phi = \chi_1$ of the side chain of residue 8 of the protein FKBP.[43] Using local-elevation biasing for the four ^3J-couplings of the χ_1-angle, this torsional angle sampled the complete range of $(0°, 360°)$, upper left panel in Figure 7. For no combination of values of χ_1 could all four ^3J-couplings be reproduced to within $\Delta Q^{\text{fb}} = 1$ Hz of the above mentioned target values Q°. Instead there was a continual increase of the local-elevation biasing or restraining energy V_k^{le} for the χ_1-angle (upper middle panel in Figure 7). Thus one or more of the reported ^3J-coupling values must be erroneous. Analysis of the available data suggested that the value $^3J_{NH_{\beta 3}} = 1.8$ Hz was probably incorrect. After removing this restraint from the restraining function,

the local-elevation potential energy did not increase with time and a range of χ_1-angle values compatible with the three target ^3J-coupling values could be identified (lower panels in Figure 7).

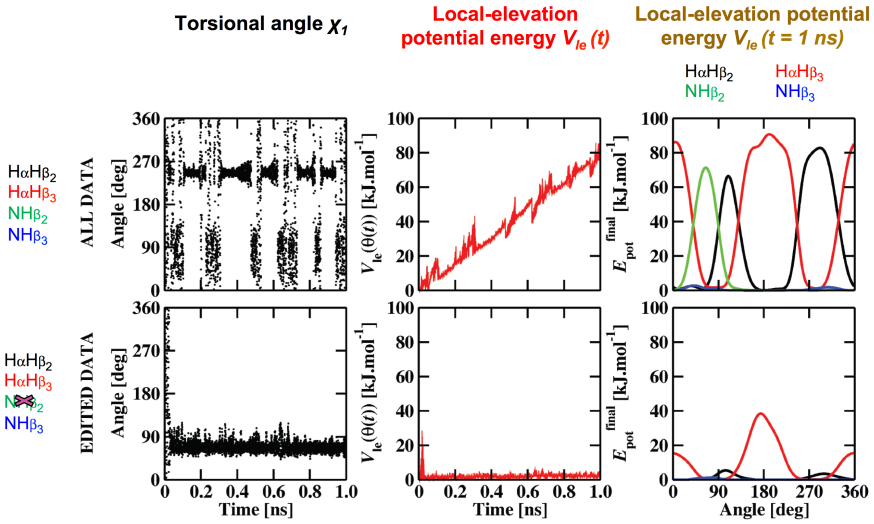

Figure 7: Detection of inconsistency of the (redundant) experimental data.[43] The torsional angle χ_1 of residue 8 of FK506 binding protein (FKBP) determines four ^3J-coupling constants. Through local-elevation search inconsistency between the four ^3J-coupling values is detected. Upper panels: four ^3J-coupling restraints. Lower panels: three ^3J-coupling restraints. Left to right: torsional angle value $\chi_1(t)$, local-elevation potential energy $V_{\mathrm{le}}(t)$, local-elevation potential energy $V_{\mathrm{le}}(\chi_1)$ at $t = 1$ ns.

Multiple-valuedness of the inverse of the function $Q(\vec{r}^N)$ may also occur for other quantities Q than ^3J-couplings or residual dipolar couplings (Table 1). The inverse of the crystallographic structure factors $F_{hkl}(\vec{r}^N)$ depends not only on the structure factor amplitudes, which are proportional to the square root of the scattering intensities I_{hkl}, but also on the phases ϕ_{hkl}. The phases cannot be experimentally measured and are instead inferred from a proposed model. The uncertainty with respect to the phases ϕ_{hkl} implies that different structures, i.e. electron densities, may map onto the same structure factor amplitudes, leading

693 to multiple-valuedness of the relation $\vec{r}^N(I_{hkl})$.

694 The question why and in which cases local-elevation biased sampling is bet-
695 ter than instantaneous restraining as applied in single-structure refinement has
696 been discussed in Ref. 44. It is summarised in Figure 8 for a one-dimensional
697 system with $Q(x)$ and $V^{\mathrm{phys}}(x)$. $V^{\mathrm{phys}}(x)$, the molecular model or force field
698 used in the MD simulation, is represented by the dashed line, and the real,
699 correct potential energy surface of the system $V^{\mathrm{real}}(x)$ by the solid line. Three
700 MD sampling techniques are compared, (i) free MD, that is using V^{phys} without
701 any restraining function $V^{Q,\mathrm{restr}}$, (ii) instantaneous restraining (IR) MD using
702 $V^{Q,\mathrm{restr}}$ but without accounting for averaging, so equivalent to single-structure
703 refinement, and (iii) local-elevation (LE) sampling MD using $V^{Q,\mathrm{restr}}$ inclusive
704 averaging as described above. Depending on the levels of the different energy
705 wells of $V^{\mathrm{phys}}(x)$ and $V^{\mathrm{real}}(x)$ and the height of the barriers between them
706 in relation to the kinetic energy $k_{\mathrm{B}}T$ available to the coordinate x in an MD
707 simulation, the different sampling techniques succeed or fail sampling the config-
708 urations x matching $\langle Q\rangle$. In free MD without restraints, the simulation may fail
709 to sample configurations with appropriate weight due to limitations in the force
710 field or molecular model (upper middle and lower left panels). Instantaneous
711 restraining or single-structure refinement may fail when different configurations
712 x contribute to the average $\langle Q\rangle$ such that $\langle Q\rangle = Q(x)$ corresponds to a configu-
713 ration x with a high energy $V^{\mathrm{phys}}(x)$ or $V^{\mathrm{real}}(x)$ (right-hand panels in Figure 8).
714 Only local-elevation MD sampling yields ranges of configurations that reproduce
715 $\langle Q\rangle$ and are of low energy V^{phys}.

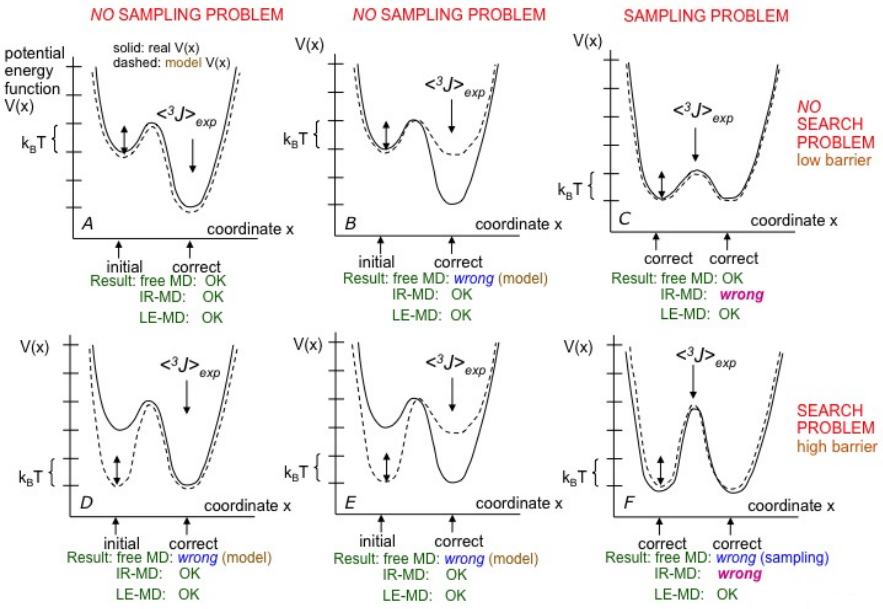

Figure 8: Schematic representation of six different real (solid line) and model (dashed line) potential energy functions illustrating the force-field problem of unrestrained MD simulations (examples B, D, E), the sampling problem of MD simulations which occurs when instantaneous restraints are applied (examples C and F), and the search problem of MD simulations due to high-energy barriers between different conformations (examples D, E, F). The double arrow indicates the thermal energy ($\frac{1}{2}k_BT$) associated with the degree of freedom x. If the thermal energy is comparable to the barrier height, transitions are easy, whereas a higher barrier leads to rare transitions. If the measured ^3J-value, $\left\langle {}^3J \right\rangle_{\mathrm{exp}}$, corresponds according to the non-linear Karplus relation to a torsional-angle coordinate x for which the potential energy is larger (examples C and F), instantaneous restraining will lead to an unrealistic configuration x.

2.10 Boltzmann sampling or weighting of configurations

It follows from statistical mechanics that a set of molecular configurations should approximate a statistical-mechanical ensemble, e.g. a Boltzmann-weighted set of structures approximating at constant temperature a canonical ensemble. The weights of the individual structures or configurations $\vec{r}^N$ should be proportional to $\exp(-V^{\mathrm{real}}(\vec{r}^N)/(k_{\mathrm{B}}T))$. Unfortunately, the real potential energy function

of a biomolecular system is not known. At the atomic level of resolution it can be approximated by a model function or force field $V^{\mathrm{phys}}(\vec{r}^N)$, and the weights of a set of structures or conformations should then be proportional to $\exp(-V^{\mathrm{phys}}(\vec{r}^N)/(k_{\mathrm{B}}T))$. Using Monte Carlo simulation or MD simulation at constant temperature this relative weighting of trajectory structures is well approximated. Yet, for most biomolecular structures reported in the literature and deposited in structural data banks, this Boltzmann weighting is not achieved. Normally such structures result from energy minimisation or temperature annealing single-structure refinement procedure, which by definition are not Boltzmann weighted. Such sets of structures do not constitute an experimental ensemble. In fact, structures based directly on experimental data should not be called an ensemble, because their relative weights do not correspond to or even approximate a well defined statistical-mechanical ensemble. For this reason it is also inappropriate to use protein structures deposited in the Protein Data Bank (PDB) as a means to directly calibrate parameters for use in a biomolecular force field. The variation in bond angles for example, represents the variation in the minimum energy position between models, not the variation which would be expected due to thermal motion.

3 What should be avoided when deriving structural information from measured data ?

The considerations in the previous sections lead to a number of choices and procedures that are to be avoided when deriving structural information from measured data for biomolecular systems.

1. Use of derived "experimental" data in the biasing or restraining function

$V^{Q,\mathrm{restr}}$. Unless the procedure f (Eq. 5) that converts measured values $\left\langle Q^{\mathrm{obs}}\right\rangle_{\mathrm{exp}}$ of an observable quantity Q^{obs} into derived values of a non-observable quantity Q^{der} involves well founded assumptions and does not increase the uncertainty of the values Q^{der}, derived data should be avoided.

2. Use of a poor molecular model or force field, e.g. without electrostatic interaction terms or without explicit solute-solvent interactions. The quality of the force field is particularly important in situations where the number of independent experimental values Q^{exp} is small compared to the number of degrees of freedom of the system.

3. Use of poorly defined experimental data or Q^{exp} values beset with a large uncertainty in a restraining function $V^{Q,\mathrm{restr}}$. In some cases the effects of uncertainty in the experimental data can be accounted for by using a flat-bottom potential energy term for restraining the range of which corresponds to the uncertainty.

4. The use of any relation $Q(\vec{r}^N)$ between an observable Q and structure $\vec{r}^N$ for which the inverse function $\vec{r}^N(Q)$ is multiple-valued without an appropriate sampling technique such as local-elevation. This applies not only to ^3J-coupling restraints, but also to restraints based on e.g. Residual Dipolar Couplings or crystallographic structure factor amplitudes.

5. Use of instantaneous restraining or single-structure refinement, unless it is *a priori* clear that the system of interest adopts a single conformation.

6. Use of a too large force constant K^{Qr} or weight of the restraining potential energy term $V^{Q,\mathrm{restr}}$ compared to the physical potential energy V^{phys}.

7. Use of molecule averaging in restraining without using a statistical-mechanically based weighting criterion, e.g. canonical or microcanonical.[122] For example, the use of replica-exchange protocols between concurrently simulated copies of the molecular system may ensure correct weighting.

8. Use of a poor or a non-Boltzmann sampling algorithm to generate a set of structures.

We note that these issues play a role when deriving structure from measured values of all observables mentioned in the Introduction and that these issues still play a role in contemporary structure determination.[123–125] It depends on the information density of the particular measurement technique, that is the ratio of the number of independent measured values Q^{exp} and the number of degrees of freedom of the molecule whose structure is to be determined, how much the choices made in the structure refinement procedure will influence the resulting molecular structure. The majority of the measurement techniques mentioned in the Introduction yield a rather low information density, which means that the structures modelled based on the experimental data will be dominated by the choice of molecular model and refinement techniques and parameters.

4 Flawed structural interpretation of measured data due to inappropriate choices made when deriving structure from experimental data

Since many structures reported in the literature have been derived based on procedures and assumptions that ideally should be avoided, one might wonder to what extent biomolecular structures that result from adhering to the standards

listed in the previous section lead to a different structural interpretation of the experimental data. This, of course, will depend on a variety of factors involved in the structure derivation, the type of molecules considered and the type of experimental data available. Below, a few examples from the literature are presented to illustrate potential consequences.

Structures of the 16-residue C-terminal half GCN4p16-31 of the leucine zipper GCN4 were derived on the basis of 172 NOE atom-atom distance bounds and 15 $^3J_{H_N H_\alpha}$-couplings measured by NMR.[44, 121] Single-structure refinement using the program X-PLOR based on (*i*) 172 NOE distance restraints, (*ii*) 14 α-helical hydrogen bond restraints (2 per hydrogen bond) between the peptide H and N atoms of residue $i + 4$ and the carbonyl oxygen of residue i with $i = 18 - 24$, and (*iii*) 8 backbone ϕ-angle restraints for residues 17-24, led to a set of 20 NMR model structures through simulated annealing.[126] However, this set of NMR model structures showed five NOE bound violations larger than 0.05 nm and two ^3J-coupling deviations larger than 3 Hz. It was decided, therefore to perform local-elevation MD time-averaging structure refinement using the GROMOS program[109] and the GROMOS force field 53A6[127] based on (*i*) the 172 NOE distance restraints using time-averaging and (*ii*) the 15 $^3J_{H_N H_\alpha}$-couplings using local-elevation sampling.[44] This led to a greater variability between the structures but overall the deviations from the experimental data were smaller: no NOE bound violations beyond 0.03 nm and no ^3J-coupling deviations larger than 1 Hz. The network of polar side chain contacts in the LE-MD structural ensemble was more extensive than in the set of NMR model structures obtained through single-structure refinement using X-PLOR. This is likely to be due to the force field used lacking electrostatic and hydrogen bonding terms.[121] In

other words, this set of 20 NMR model structures, deposited in the Protein Data Bank, does not capture the expected contacts between the polar side chains of the helix. In this case an inappropriate choice of hydrogen-bond and torsional-angle restraints based on values of derived, non-observable quantities Q^{der}, the neglect of averaging by applying instantaneous restraining or single-structure refinement, and the use of a force field without electrostatic interaction terms led to a set of structures with a lower structural variability than indicated by the measured data, and thus not only to a poor set of structural models but to the misinterpretation of the data on which these models were based.

An example of the combined effect of inaccuracies of the force field used in single-structure refinement and a limited set of atom-atom distance bounds derived from NMR data can be found in Ref. 128. Although the proposed structure of the complex of the barley lipid transfer protein 1 (LTP) in complex with the fatty acid ligand palmitate was based on the use of 25 protein-ligand NOE restraints,[128] these were not sufficient to identify the details of the ligand binding site using the calculation protocol applied. Indeed, MD simulation starting from the NMR model structure indicated this structure was not stable. The palmitate ligand moved out of the internal cavity and became exposed to solvent.[129] Using different sets of restraints (omitting hydrogen-bond restraints), different protonation states and force-field parameters two alternative palmitate binding modes characterised by different hydrogen-bonding patterns, were identified for palmitate.[129] The two modes have similar protein-ligand interaction energies suggesting that both are significantly populated. In these binding modes the palmitate head group is not involved in a salt bridge or hydrogen bond to the side chain of Cys 9 as had been previously suggested.[128] Instead the ligand

formed hydrogen bonds with main-chain amide groups of residues in helix A. The ligand binding exploits irregularities in the helical hydrogen-bonding pattern in this helix due to the presence of Pro 12. Simulations of single mutant P12V and double mutant P12V,P20V variants of barley LTP also suggested that the presence of Proline at position 12 in helix A is needed to stabilize the binding of palmitate to barley LTP.

Another example of the incomplete picture of ligand binding based on X-ray and NMR data as obtained by single-structure refinement based on a limited set of experimental data can be found in Ref. 130. The data suggested the occurrence of two ligand binding modes of the ligand caprate to maize LTP. Using different protonation states and configurational sampling strategies MD simulation[131] indicated that one particular binding mode (M) is preferred in maize LTP rather than a mixture of two different binding modes (M and B) suggested previously. The mobility of the caprate ligand explained the absence of electron density for the ligand head group in the X-ray structure determination.[132]

Currently the study of so-called intrinsically disordered proteins is rather popular. For such proteins the ratio of the amount of independent data that can be accurately measured compared to the number of protein configurational degrees of freedom that allow for disorder is very, very low. This implies that the reliability of the generated structures is almost entirely determined by the combination of molecular model and force field used in the structure generation rather than by the measured data. This applies to most of the observable quantities and measurement techniques mentioned in the Introduction.

Even when using a high information density technique such as X-ray diffraction crystallography the interpretation of the electron density of a molecule may

be flawed by ignoring the motion of atoms in the structure refinement process. This is illustrated by a time-averaging structure factor amplitude restraining MD simulation of the protein basic pancreatic trypsin inhibitor (BPTI).[87] The X-ray model structure derived using single-structure refinement based on X-ray diffraction data contained four internal water molecules without contact to bulk solvent due to the presence of the side chain of Glu 7 blocking their access to the protein surface. Allowing for averaging through the time-averaging structure refinement procedure it was found that the electron density at the proposed position of the Glu 7 side chain could be due to a water molecule. While the side chain actually does not have its own well-defined electron density, it exists in many different conformations during the time-averaging refinement-simulation.[87] These conformations are consistent with the crystallographic data, because no significant density difference exists. In contrast to the single-structure refinement result, the new water site bridges the four internal water sites to the bulk water outside. Other examples of misinterpretation of experimental data can be found in Ref. 79–81, 133, 134. The risk of misinterpretation of experimental data is even higher for the measurement techniques of low information density mentioned in the Introduction.

5 Pollution of structural databases by flawed structures

During the past years, a number of protein structures deposited in the Protein Data Bank (PDB) were corrected or retracted, because the interpretation of the corresponding X-ray diffraction data was flawed.[79, 80] Considering the number of things that can go wrong in the process of structure refinement,[81, 135, 136] the number of partially flawed or non-optimal structures is likely to be large.[81]

This highlights the importance of being able to correct structures deposited in the PDB as more robust procedures to derive structure from measured values of observable quantities[134] or to check the derived structures with respect to geometric and energetic criteria[81] become available and especially when these result in a better match to the measured values of observables[137] than existing structures. It also highlights the need for all structures to be deposited together with values of the observables such as NOE bounds, ^3J-couplings and structure factor amplitudes, force fields and computational protocols used for their generation. The primary criteria for whether a structure is included in these critical public databases must be the extent to which the models can account for the available experimental data. Limiting the ability of researchers other than the original depositors to correct structures will lead to the progressive pollution of the PDB with partially flawed structures. Structures should be stored independently of the observed data from which they were derived, and the key choices and procedures of the structural derivation should be deposited with the structures. Recent moves by the PDB and other repositories to enforce this should be encouraged.[138]

In fact, the quality of structures is an on-going concern to the PDB, and the PDB has held a series of meetings to address concerns regarding the deposition of flawed structures.[139] While the ease with which data can be acquired has increased and data processing has improved, the extent to which partially automated tools are used by less experienced persons to solve larger structures has led to flawed structures.[140] Solving structures for more complex systems even with modern tools can be just as challenging (i.e. error prone) as for simpler systems with older tools. For MD simulation, the quality of force fields and

sampling has improved, but so has the complexity of the systems studied. It would be very wrong to assume all recent simulation studies are of high quality.

6 Conclusion

The process of deriving structural information from measured data for biomolecular systems is a complex one involving many assumptions and approximations. These may introduce uncertainty or error in the derived structures, which in turn may then misrepresent reality. This may be avoided by carefully considering the various choices to be made in the refinement process. These considerations regard many types of observables and measurement techniques, not only NMR spectroscopy, but also X-ray and neutron diffraction, small-angle and wide-angle X-ray scattering, free-electron laser imaging, cryo-electron microscopy, EPR, Infrared and Raman spectroscopy, CD, FRET, ATM and ion-mobility mass spectrometry. The lower the information density of a measurement technique, the larger will be the chance that problematic choices of approximations and parameters of the structure refinement process will go undetected.

Due to the complexity of the process of deriving structures from experimentally measured data and the different characteristics of the variety of experimental data that can be used, it is not possible to assert what is "best practice" and expect this to be applicable to all cases. What procedure to choose will depend on (*i*) the type, quality and number of experimental data, (*ii*) the relationship between these data and structure, (*iii*) the choice of the degrees of freedom of the molecular model used, (*iv*) the quality of the molecular model and force field used, (*v*) the range of the model parameter values that is sampled, and (*vi*) the extent of configurational sampling and biasing executed. While it would of

course be nice to have a straightfoward checklist for determining structure quality, the factors at play and their relative importance are likely to vary on a case-by-case basis, thus such a list will always be a simplification and likely to lead to even further problems. Unfortunately, a high-dimensional problem often only has a high-dimensional answer.

7 Acknowledgements

This work was financially supported by grant No 20020-137827 of the Swiss National Science Foundation and by grant No 228076 of the European Research Council (ERC), which is gratefully acknowledged.

References

[1] J. C. Kendrew, G. Bodo, H. M. Dintzis, R. G. Parrish, H. Wyckoff, D. C. Phillips, *Nature* **1958**, 181, 662-666

[2] C. C. F. Blake, D. F. Koenig, G. A. Mair, A. C. T. North, D. C. Phillips, V. R. Sarma, *Nature* **1965**, 206, 757-761

[3] J. Drenth, C. M. Enzing, K. H. Kalk, J. C. A. Vessies, *Nature* **1976**, 264, 373-377

[4] A. Wlodawer, J. Walter, R. Huber, L. Sjölin, *J. Mol. Biol.* **1984**, 180, 301-329

[5] D. I. Svergun, M. H. J. Koch, *Rep. Prog. Phys.* **2003**, 66, 1735-1782

[6] K. J. Gaffney, H. N. Chapman, *Science* **2007**, 316, 1444-1448

[7] M. Walczak, H. Grubmüller, *Phys. Rev. E* **2014**, 90, 022714

[8] X.-C. Bai, G. McMullan, S. H. W. Scheres, *Trends Biochem. Sci.* **2015**, 40, 49-57

[9] R. R. Ernst, G. Bodenhausen, A. Wokaun, *Principles of Nuclear Magnetic Resonance in One and Two Dimensions*, Clarendon Press, Oxford, England, **1990**

[10] K. D. Berndt, P. Güntert, L. P. M. Orbons, K. Wüthrich, *J. Mol. Biol.* **1992**, 227, 757-775

[11] C. C. Jao, B. G. Hegde, J. Chen, I. S. Haworth, R. Langen, *Proc. Natl. Acad. Sci. USA* **2008**, 105, 19666-19671

[12] S. Bagchi, S. G. Boxer, M. D. Fayer, *Phys. Chem. B* **2012**, 116, 4034-4042

[13] Y. Hong, L. Meng, S. Chen, C. W. T. Leung, L.-T. Da, M. Faisal, D.-A. Silva, J. Liu, J. W. Y. Lam, X. Huang, B. Z. Tang, *J. Am. Chem. Soc.* **2012**, 134, 1680-1689

[14] C. A. E. Hauser, R. Deng, A. Mishra, Y. Loo, U. Khoe, F. Zhuang, D. W. Cheong, A. Accardo, M. B. Sullivan, C. Riekel, J. Y. Ying, U. A. Hauser, *Proc. Natl. Acad. Sci. USA* **2011**, 108, 1361-1366

[15] M. Hoefling, N. Lima, D. Haenni, C. A. M. Seidel, B. Schuler, H. Grubmüller, *PLoS ONE* **2011**, 6, e19791

[16] M. M. Reif, C. Oostenbrink, *J. Comput. Chem.* **2014**, 35, 2319-2332

[17] A. T. Brunger, P. Strop, M. Vrljic, S. Chu, K. R. Weninger, *J. Struct. Biol.* **2011**, 173, 497-505

[18] T. Ando, *Nanotechnology* **23**, 062001

[19] Z. Hall, A. Politis, M. F. Bush, L. J. Smith, C. V. Robinson, *J. Am. Chem. Soc.* **2012**, 134, 3429-3438

[20] J. Drenth, *Principles of Protein X-ray Crystallography*, Springer, New York, USA, **1994**

[21] R. Boelens, T. M. G. Koning, R. Kaptein, *J. Mol. Struct.* **1988**, 173, 299-311

[22] M. Karplus, *J. Chem. Phys.* **1959**, 30, 11-15

[23] D. Steiner, J. R. Allison, W. F. van Gunsteren, *J. Biomol. NMR* **2012**, 53, 223-246

[24] B. Han, Y. Liu, S. W. Ginzinger, D. S. Wishart, *J. Biomol. NMR*, **2011**, 50, 43-57

[25] W. F. van Gunsteren, A. M. J. J. Bonvin, X. Daura, L. J. Smith, in: *Structure Computation and Dynamics in Protein NMR, Biol. Magnetic Resonance Vol. 17* (Eds.: R. N. Krishna and L. J. Berliner), Plenum Publishers, New York, USA, **1999**, pp. 3-35.

[26] J. H. Lee, F. Li, A. Grishaev, A. Bax *J. Am. Chem. Soc.*, **2015**, 137, 1432-1435

[27] U. Stocker, D. Juchli, W. F. van Gunsteren, *Mol. Sim.*, **2003**, 29, 123-138

[28] A. T. Brünger, *X-PLOR. A System for X-ray Crystallography and NMR*, Yale University Press, New Haven, CT, USA, **1992**.

[29] W. A. Hendrickson, J. H. Konnert, in: *Biomolecular Structure, Conformation, Function and Evolution, Volume 1: Diffraction and Related Studies* (Ed.: R. Srinivasan), Pergamon, Oxford, U.K., **1981**, pp. 43-57.

[30] W. F. van Gunsteren, R. Kaptein, E. R. P. Zuiderweg, in: *Proceedings NATO/CECAM workshop on nucleic acid conformation and dynamics* (Ed.: W.K. Olson), CECAM, Orsay, France, **1984**, pp. 79-92.

[31] R. Kaptein, E. R. P. Zuiderweg, R. M. Scheek, R. Boelens, W. F. van Gunsteren, *J. Mol. Biol.* **1985**, 182, 179-182

[32] A. T. Brünger, J. Kuriyan, M. Karplus, *Science* **1987**, 235, 458-460

[33] M. Fujinaga, P. Gros, W. F. van Gunsteren, *J. Appl. Cryst.* **1989**, 22, 1-8

[34] G. F. Schröder *Curr. Opin. Struct. Biol.* **2015**, 31, 20-27

[35] H. M. Berman, J. Westbrook, Z. Feng, G. Gilliland, T. N. Bhat, H. Weissig, I. N. Shindyalov, P. E. Bourne, *Nucleic Acids Res* **2000**, 28, 235-242

[36] W. F. van Gunsteren, J. Dolenc, A. E. Mark, *Curr. Opin. Struct. Biology* **2008**, 18, 149-153

[37] A. Glättli, W. F. van Gunsteren, *Angew. Chem.* **2004**, 116, 6472-6476; *Angew. Chem. Int. Ed.* **2004**, 43, 6312-6316

[38] K. Gademann, A. Häne, M. Rueping, B. Jaun, D. Seebach, *Angew. Chem.* **2003**, 115, 1573-1575; *Angew. Chem. Int. Ed.* **2003**, 42, 1534-1537

[39] B. Zagrovic, G. Jayachandran, I. S. Millett, S. Doniach, V. S. Pande, *J. Mol. Biol.* **2005**, 353, 232-241

[40] B. Zagrovic, W. F. van Gunsteren, *Proteins Struct. Funct. Bioinf.* **2006**, 63, 210-218

[41] W. F. van Gunsteren, R. Bürgi, C. Peter, X. Daura, *Angew. Chem.* **2001**, 113, 363-367; *Angew. Chem. Int. Ed.* **2001**, 40, 351-355

[42] W. F. van Gunsteren, D. Bakowies, R. Baron, I. Chandrasekhar, M. Christen, X. Daura, P. Gee, D. P. Geerke, A. Glättli, P. H. Hünenberger, M. A. Kastenholz, C. Oostenbrink, M. Schenk, D. Trzesniak, N. F. A. van der Vegt, H.B. Yu, *Angew. Chem.* **2006**, 118, 4168-4198; *Angew. Chem. Int. Ed.* **2006**, 45, 4064-4092

[43] J. R. Allison, W. F. van Gunsteren, *ChemPhysChem* **2009**, 10, 3213-3228

[44] J. Dolenc, J. H. Missimer, M. O. Steinmetz, W. F. van Gunsteren, *J. Biomol. NMR* **2010**, 47, 221-235

[45] B. Vögeli, J. Ying, A. Grishaev, A. Bax, *J. Am. Chem. Soc.* **2007**, 129, 9377-9385

[46] A. Pardi, M. Billeter, K. Wüthrich, *J. Mol. Biol.* **1984**, 180, 741-751

[47] R. Brüschweiler, D. A. Case, *J. Am. Chem. Soc.* **1994**, 116, 11199-11200

[48] A. C. Wang, A. Bax, *J. Am. Chem. Soc.* **1996**, 118, 2483-2494

[49] J. M. Schmidt, M. Blümel, F. Löhr, H. Rüterjans, *J. Biomol. NMR* **1999**, 14, 1-12

[50] A. DeMarco, M. Linàs, K. Wüthrich, *Biopolymers* **1978**, 17, 617-636

[51] A. DeMarco, M. Linàs, K. Wüthrich, *Biopolymers* **1978**, 17, 2727-2742

[52] R. J. Abraham, K. A. McLauchlan, *Mol. Phys.* **1962**, 5, 513-523

[53] C. M. Deber, E. R. Blout, D. A. Torchia, *J. Am. Chem. Soc.* **1971**, 93, 4893-4897

[54] M. T. Cung, M. Marraud, J. Nèel, in: *10th Prague IUPAC Micro-Symposium on Macromolecules*, Prague, **1972**, p. C-3.

[55] A. J. Fischman, D. H. Live, H. R. Wyssbrod, W. C. Agosta, D. Cowburn, *J. Am. Chem. Soc.* **1980**, 102, 2533-2539

[56] C. Pérez, F. Löhr, H. Rüterjans, J. M. Schmidt, *J. Am. Chem. Soc.* **2001**, 123, 7081-7093

[57] X. Daura, I. Antes, W. F. van Gunsteren, W. Thiel, A. E. Mark, *Proteins Struct. Funct. Genet.* **1999**, 36, 542-555

[58] T. S. Harvey, W. F. van Gunsteren, in: *Techniques in Protein Chemistry IV*, Academic Press, **1993**, pp. 615-622.

[59] D. A. Case, *Curr. Opin. Struct. Biol.* **2013**, 23, 172-176

[60] W. F. van Gunsteren, R. Boelens, R. Kaptein, R. M. Scheek, E. R. P. Zuiderweg, in: *Molecular Dynamics and Protein Structure* (Ed.: J. Hermans), Polycrystal Book Service, P.O. Box 27, Western Springs, Ill. 60558, USA, **1985**, pp. 92-99.

[61] J. de Vlieg, R. Boelens, R. M. Scheek, R. Kaptein, W. F. van Gunsteren, *Isr. J. Chem.* **1986**, 27, 181-188

[62] A. E. Torda, R. M. Brunne, T. Huber, H. Kessler, W. F. van Gunsteren, *J. Biomol. NMR* **1993**, 3, 55-66

[63] K. Wüthrich, M. Billeter, W. Braun, *J. Mol. Biol.* **1983**, 169, 949-961

[64] W. F. van Gunsteren, S. R. Billeter, A. A. Eising, P. H. Hünenberger, P. Krüger, A. E. Mark, W. R. P. Scott, I. G. Tironi, Biomolecular Simulation: The GROMOS96 Manual and User Guide, Vdf Hochschulverlag AG an der ETH Zürich, Zürich, Switzerland, **1996**.

[65] C. M. Fletcher, D. N. M. Jones, R. Diamond, *J. Biomol. NMR* **1996**, 8, 292-310

[66] M. Nilges, *Proteins* **1993**, 17, 297-309

[67] M. Nilges, M. J. Macias, S. I. O'Donoghue, H. Oschkinat, *J. Mol. Biol.* **1997**, 269, 408-422

[68] W. F. van Gunsteren, in: *Studies in Physical and Theoretical Chemistry, Vol 71, Modelling of Molecular Structures and Properties* (Ed.: J.-L. Rivail), Elsevier, Amsterdam, **1990**, pp. 463-478.

[69] A. D. Kline, W. Braun, K. Wüthrich, *J. Mol. Biol.* **1988**, 204, 675-724

[70] G. M. Clore, A. T. Brünger, M. Karplus, A. M. Gronenborn, *J. Mol. Biol.* **1986**, 191, 523-551

[71] G. M. Clore, D. K. Sukumaran, M. Nilges, J. Zarbock, A. M. Gronenborn, *EMBO J.* **1987**, 6, 529-537

[72] G. M. Clore, A. M. Gronenborn, M. Nilges, D. K. Sukumaran, J. Zarbock, *EMBO J.* **1987**, 6, 1833-1842

[73] G. M. Clore, A. M. Gronenborn, M. Nilges, C. A, Ryan, *EMBO J.* **1987**, 26, 8012-8023

[74] G. M. Clore, D. K. Sukumaran, M. Nilges, A. M. Gronenborn, *Biochemistry* **1987**, 26, 1732-1745

[75] G. M. Clore, M. Nilges, D. K. Sukumaran, A. T. Brünger, M. Karplus, A. M. Gronenborn, *EMBO J.* **1986**, 5, 2729-2735

[76] W. F. van Gunsteren, M. Karplus, *Macromolecules* **1982**, 15, 1528-1544

[77] J. Hermans, H. J. C. Berendsen, W. F. van Gunsteren, J. P. M. Postma, *Biopolymers* **1984**, 23, 1513-1518

[78] B. R. Brooks, R. E. Bruccoleri, B. D. Olafson, D. J. States, S. Swaminathan, M. Karplus, *J. Comput. Chem.* **1983**, 4, 187-217

[79] A. M. Davis, S. A. St-Gallay, G. J. Kleywegt, *Drug Disc. Today* **2008**, 13, 831-841

[80] J. Agirre, G. Davis, K. Wilson, K. Cowtan, *Nature Chem. Biol.* **2015**, 11, 303

[81] W. G. Touw, R. P. Joosten, G. Vriend, *J. Mol. Biol.* **2016**, 428, 1375-1393

[82] C. A. Schiffer, R. Huber, K. Wüthrich, W. F. van Gunsteren, *J. Mol. Biol.* **1994**, 241, 588-599

[83] A. E. Torda, R. M. Scheek, W. F. van Gunsteren, *Chem. Phys. Lett.* **1989**, 157, 289-294

[84] P. Gros, W. F. van Gunsteren, W. G. J. Hol, *Science* **1990**, 249, 1149-1152

[85] P. Gros, W. F. van Gunsteren, *Mol. Sim.* **1993**, 10, 377-395

[86] C. A. Schiffer, P. Gros, W. F. van Gunsteren, *Acta Cryst. D* **1995**, 51, 85-92

[87] C. A. Schiffer, W. F. van Gunsteren, *Proteins Struct. Funct. Bioinf.* **1999**, 36, 501-511

[88] W. R. P. Scott, A. E. Mark, W. F. van Gunsteren, *J. Biomol. NMR* **1998**, 12, 501-508

[89] N. Hansen, F. Heller, N Schmid, W. F. van Gunsteren, *J. Biomol. NMR* **2014**, 60, 169-187

[90] D. A. Pearlman, P. A. Kollman, *J. Mol. Biol.* **1991**, 220, 457-479

[91] U. Schmitz, A. Kumar, T. L. James, *J. Am. Chem. Soc.* **1992**, 114, 10654-10656

[92] U. Schmitz, B. Ulyanov, A. Kumar, T. L. James, *J. Mol. Biol.* **1993**, 234, 373-389

[93] D. A. Pearlman, *J. Biomol. NMR* **1994**, 4, 1-16

[94] D. A. Pearlman, *J. Biomol. NMR* **1994**, 4, 279-299

[95] A. P. Nanzer, W. F. van Gunsteren, A. E. Torda, *J. Biomol. NMR* **1995**, 6, 313-320

[96] A. P. Nanzer, A. E. Torda, C. Bisang, C. Weber, J. A. Robinson, W. F. van Gunsteren, *J. Mol. Biol.* **1997**, 267, 1012-1025

[97] A. P. E. Kunz, J. R. Allison, D. P. Geerke, B. A. C. Horta, P. H. Hünenberger, S. Riniker, N. Schmid, W. F. van Gunsteren, *J. Comput. Chem.* **2012**, 33, 340-353

[98] R. M. Scheek, A. E. Torda, J. Kemmink, W. F. van Gunsteren, in: *Computational Aspects of the Study of Biological Macromolecules by Nuclear Magnetic Resonance Spectroscopy* (Eds.: J. C. Hoch, F. M. Poulsen, C. Redfield), NATO ASI Series A225, Plenum Press, New York, USA, **1991**, pp. 209-217.

[99] J. Fennen, A. E. Torda, W. F. van Gunsteren, *J. Biomol. NMR* **1995**, 6, 163-170

[100] T. Huber, W. F. van Gunsteren, *J. Phys. Chem. A* **1998**, 102, 5937-5943

[101] B. Hess, R. M. Scheek, *J. Magn. Reson.* **2003**, 164, 19-27

[102] J. W. Pitera, J. D. Chodera, *J. Chem. Theory Comput.* **2012**, 8, 4335-3451

[103] B. Roux, J. Weare, *J. Chem. Phys.* **2013**, 138, 084107

[104] A. Cavalli, C. Camilloni, M. Vendruscolo, *J. Chem. Phys.* **2013**, 138, 094112

[105] S. Olsson, J. Frellsen, W. Boomsma, K. V. Mardia, T. Hamelryck, *PLoS One* **2013**, 8, e79439

[106] Y. Sugita, Y. Okamoto, *Chem. Phys. Lett.* **1999**, 314, 141-151

[107] Y. Sugita, A. Kitao, Y. Okamoto, *J. Chem. Phys.* **2000**, 113, 6042-6051

[108] H. Fukunishi, O. Watanabe, S. Takada, *J. Chem. Phys.* **2002**, 116, 9058-9067

[109] N. Schmid, J. R. Allison, J. Dolenc, A. P. Eichenberger, A.-P. E. Kunz, W. F. van Gunsteren, *J. Biomol. NMR* **2011**, 51, 265-281

[110] W. Rieping, M. Habeck, M. Nilges, *Science* **2005**, 309, 303-306

[111] X. Daura, K. Gademann, B. Jaun, D. Seebach, W. F. van Gunsteren, A. E. Mark, *Angew. Chem.* **1999**, 111, 249-253; *Angew. Chem. Int. Ed.* **1999**, 38, 236-240

[112] A. E. Torda, R. M. Scheek, W. F. van Gunsteren, *J. Mol. Biol.* **1990**, 214, 223-235

[113] C. A. Schiffer, R. Huber, K. Wüthrich, W. F. van Gunsteren, *J. Mol. Biol.* **1994**, 241, 588-599

[114] D. Seebach, P. E. Ciceri, M. Overhand, B. Jaun, D. Rigo, L. Oberer, U. Hommel, R. Amstutz, H. Widmer, *Helv. Chim. Acta* **1996**, 79, 2043-2066

[115] D. Seebach, S. Abele, K. Gademann, G. Guichard, T. Hintermann, B. Jaun, J. L. Matthews, J. V. Schreiber, L. Oberer, U. Hommel, H. Widmer, *Helv. Chim. Acta* **1998**, 81, 932-982

[116] D. Seebach, K. Gademann, J. V. Schreiber, J. L. Matthews, T. Hintermann, B. Jaun, L. Oberer, U. Hommel, H. Widmer, *Helv. Chim. Acta* **1997**, 80, 2033-2038

[117] T. Huber, A. E. Torda, W. F. van Gunsteren, *J. Comput.-Aided Mol. Design* **1994**, 8, 695-708

[118] A. Laio, M. Parrinello, *Proc. Natl. Acad. Sci. USA* **2002**, 99, 12562-12566

[119] M. Christen, B. Keller, W. F. van Gunsteren, *J. Biomol. NMR* **2007**, 39, 265-273

[120] Z. Gattin, J. Zaugg, W. F. van Gunsteren, *ChemPhysChem* **2010**, 11, 830-835

[121] J. H. Missimer, J. Dolenc, M. O. Steinmetz, W. F. van Gunsteren, *Prot. Sci.* **2010**, 19, 2462-2474

[122] Z. Lin, W. F. van Gunsteren, *J. Chem. Phys.* **2015**, 143, 034110

[123] A. Kuzmanic, N. S. Pannu, B. Zagrovic, *Nat. Commun.* **2014**, 5, 3220

[124] Z. Dauter, A. Wlodawer, W. Minor, M. Jaskolski, B. Rupp, *IUCrJ* **2014**, 1, 179-193

[125] H. van den Bedem, J. S. Fraser, *Nat. Meth.* **2015**, 12, 307-318

[126] M. O. Steinmetz, I. Jelesarov, W. M. Matousek, S. Honnappa, W. Jahnke, J. H. Missimer, S. Frank, A. T. Alexandrescu, R. A. Kammerer *Proc. Natl. Acad. Sci. USA* **2007**, 104, 7062-7067

[127] C. Oostenbrink, A. Villa, A.E. Mark, W.F. van Gunsteren, *J. Comp. Chem.* **2004**, 25, 1656-1676

[128] M. H. Lerche, F. M. Poulsen, *Protein Sci.* **1998**, 7, 2490-2498

[129] L. J. Smith, W. F. van Gunsteren, J. R. Allison, *Protein Sci.* **2013**, 22, 56-64

[130] L. F. Pacios, C. Gómez-Casado, L. Tordesillas, A. Palacin, R. Sánchez-Monge, A. Díaz-Perales, *J. Comput. Chem.* **2012**, 33, 1831-1844

[131] L. J. Smith, Y. Roby, J. R. Allison, W. F. van Gunsteren, *Biochemistry* **2013**, 52, 5024-5038

[132] G. W. Han, J. Y. Lee, H. K. Song, C. S. Chang, K. Min, J. Moon, D. H. Shin, M. L. Kopka, M. R. Sawaya, H. S. Yuan, T. D. Kim, J. Choe, D. Lim, H. J. Moon, S. W. Suh, *J. Mol. Biol.* **2001**, 308, 263-278

[133] D. Trzesniak, W. F. van Gunsteren, *Prot. Sci.* **2006**, 15, 2544-2551

[134] B. T. Burnley, P. V. Afonine, P. D. Adams, P. Gros, *eLife* **2012**, 1, 1, e00311

[135] A. Wlodawer, W. Minor, Z. Dauter, M. Jaskolski, *FEBS Journal* **2008**, 275, 1-21

[136] A. Wlodawer, W. Minor, Z. Dauter, M. Jaskolski, *FEBS Journal* **2013**, 280, 5705-5736

[137] R. P. Joosten, K. Joosten, G. N. Murshudov, A. Perrakis, *Acta Cryst.* **2012**, D68, 484-496

[138] G. T. Montelione, M. Nilges, A. Bax, P. Güntert, T. Herrmann, J. S. Richardson, C. D. Schwieters, W. F. Vranken, G. W. Vuister, D. S. Wishart, H. M. Berman, G. J. Kleywegt, J. L. Markley, *Structure* **2013**, 21, 1563-1570

[139] P. D. Adams, K. Aertgeerts, C. Bauer, J. A. Bell, H. M. Berman, T. N. Bhat, J. M. Blaney, E. Bolton, G. Bricogne, D. Brown, S. K. Burley, D. A. Case, K. L. Clark, T. Darden, P. Emsley, V. A. Feher, Z. Feng, C. R. Groom, S. F. Harris, J. Hendle, T. Holder, A. Joachimiak, G. J. Kleywegt, T. Krojer, J. Marcotrigiano, A. E. Mark, J. L. Markley, M. Miller, W. Minor, G. T. Montelione, G. Murshudov, A. Nakagawa, H. Nakamura, A. Nicholls, M. Nicklaus, R. T. Nolte, A. K. Padyana, C. E. Peishoff, S. Pieniazek, R. J. Read, C. Shao, S. Sheriff, O. Smart, S. Soisson, J. Spurlino, T. Stouch, R. Svobodova, W. Tempel, T. C. Terwilliger, D. Tronrud, S. Velankar, S. C. Ward, G. L. Warren, J. D. Westbrook, P. Williams, H. Yang, J. Young, *Structure* **2016**, 24, 502-508

[140] G. Miller, *Science* **2006**, 314, 1856-1857